
Article:
März, C orcid.org/0000-0003-2558-4711, Riedinger, N, Sena, C et al. (1 more author) (2018) Phosphorus dynamics around the sulphate-methane transition in continental margin sediments: Authigenic apatite and Fe(II) phosphates. Marine Geology, 404. pp. 84-96. ISSN 0025-3227

https://doi.org/10.1016/j.margeo.2018.07.010

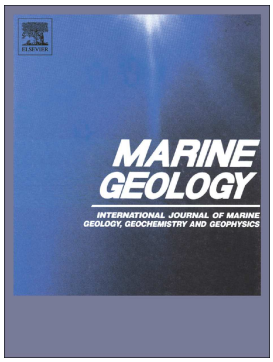

Phosphorus dynamics around the sulphate-methane transition in continental margin sediments: Authigenic apatite and Fe(II) phosphates

C. März, N. Riedinger, C. Sena, S. Kasten

PII: S0025-3227(18)30086-0
DOI: doi:10.1016/j.margeo.2018.07.010
Reference: MARGO 5825

To appear in: *Marine Geology*

Received date: 13 March 2018
Revised date: 17 July 2018
Accepted date: 22 July 2018

Please cite this article as: C. März, N. Riedinger, C. Sena, S. Kasten , Phosphorus dynamics around the sulphate-methane transition in continental margin sediments: Authigenic apatite and Fe(II) phosphates. Margo (2018), doi:10.1016/j.margeo.2018.07.010

Phosphorus dynamics around the sulphate-methane transition in continental margin sediments: Authigenic apatite and Fe(II) phosphates

C. März[1], N. Riedinger[2], C. Sena[3, 4], S. Kasten[5,6]

[1] School of Earth and Environment, University of Leeds, LS2 9JT, Leeds, UK

[2] Boone Pickens School of Geology, Oklahoma State University, Stillwater, OK, USA

[3] Centre for Environmental and Marine Studies, University of Aveiro, Portugal

[4] Department of Geosciences, University of Oslo, Oslo, Norway

[5] Alfred Wegener Institute Helmholtz Centre for Polar and Marine Research, Bremerhaven, Germany

[6] MARUM - Center for Marine Environmental Sciences and Department of Geosciences, University of Bremen, Germany

Abstract

The formation of authigenic phosphate minerals in marine sediments is an important process for the burial and long-term storage of the bio-essential nutrient phosphorus (P). In this context, we report the composition of pore waters, bulk sediments, and the speciation of P in four sediment cores recovered on the continental margins off the Amazon, Rio de la Plata and Zambezi rivers. Here, pronounced sulphate-methane transitions (SMTs) occur between 4.5 and 6.5 m sediment depth where sulphate is consumed by the anaerobic oxidation of methane and free hydrogen sulphide builds up in the pore waters. This leads to the reductive dissolution of primary Fe (oxyhydr)oxides (FeOx) by hydrogen sulphide, and the subsequent liberation of FeOx-adsorbed phosphate into pore waters at the SMT. The released phosphate

builds up to significant concentrations, making it available for the precipitation of authigenic minerals within and below the SMT. Using a sequential P extraction, we find consistently high contributions of carbonate fluorapatite (CFA) to the total P pool within the SMT, where it likely precipitates due to high local phosphate concentrations, high alkalinity and abundant dissolved Ca in the pore waters. PHREEQC calculations confirm these results, with highest saturation states with respect to authigenic apatite calculated at all SMTs. CFA authigenesis, however, is insufficient to completely consume pore water phosphate, leading to diffusive loss of phosphate from the SMT. While the upward decrease in phosphate above the SMT is relatively gentle, the significantly steeper phosphate gradient into underlying sediments suggests the formation of another authigenic mineral phase. Sequential P extraction and PHREEQC results clearly show that the dominant authigenic phase below the SMT is not CFA. Instead, geochemical conditions below the sulphidic zone at all four sites are favourable for the precipitation of Fe(II) phosphate minerals (e.g., vivianite). These conditions are summarized as the absence of sulphate and free hydrogen sulphide, but the presence of Fe^{2+} and phosphate in pore waters, and low calcium carbonate contents in the sediment. While we did not directly detect or quantify Fe(II) phosphate minerals, Fe-bound P clearly increases in the sediments below the sulphidic zones at all studied sites, and this is where highest pore water saturation states with respect to vivianite are calculated with PHREEQC. In addition, geochemical inverse models performed in PHREEQC show that vivianite formation is an important geochemical process controlling the observed patterns of dissolved P and Fe, pH and redox potential of the pore waters analysed below the SMT. We therefore argue that Fe(II) phosphate minerals are formed in these ocean margin sediments on a large scale, and pore water and sediment data indicate that this Fe-bound P largely originates from FeOx-adsorbed phosphate liberated within the sulphidic SMT. This study suggests that under specific but not unusual depositional conditions, SMTs are hotspots for biogeochemical P cycling in marginal marine sediments worldwide, with CFA precipitating within the SMT,

and Fe(II) phosphates forming below it. It also adds to the growing evidence that Fe(II) phosphates may contribute significantly to the long-term burial of reactive P phases in Fe-rich, methanic marine sediments, and thus act as a previously underestimated sedimentary P sink.

Keywords: Deep-sea fan, continental margin, iron, phosphorus, vivianite, diagenesis, sulphate-methane transition, AOM

Highlights

- Release of phosphate at sulphate-methane transitions (SMT) in continental margin sediments.
- Carbonate fluorapatite (CFA) formation within the SMT, but not below it.
- Pore water phosphate drawdown below SMT due to Fe(II) phosphate formation.
- Phosphate diagenesis controlled by fixation of SMT due to low sedimentation rate on deep-sea fans following Holocene sea level rise.

1 Introduction

Continental margins are transitional zones between land and ocean, receiving a mixture of continentally derived siliciclastic and marine biogenic material. Particularly high amounts of detrital sediments are deposited off large river mouths, often accumulating on deep-sea fans

or other continental slope depocenters. These sediments are usually rich in terrigenous Fe (oxyhydr)oxides (FeOx; e.g., ferrihydrite, goethite, hematite) that are both important sorbents of dissolved metals and phosphate, and terminal electron acceptors for microbial organic matter remineralisation (e.g., Goldberg, 1954; Froelich et al., 1979; Feely et al., 1991). Phosphate ions have a strong affinity to amorphous and poorly crystalline FeOx surfaces, which can lead to significant scavenging of phosphate from solution (e.g., Einsele, 1938; Berner, 1973; Slomp et al., 1996a; Delaney, 1998; Canfield et al., 2005). Once deposited at the seafloor and buried below the oxic zone, these FeOx are partially dissolved by dissimilatory Fe reduction (Lovley and Philips, 1988), liberating the adsorbed phosphate into the adjacent pore waters. This dissolved phosphate is either transported (by diffusion and/or advection) to the water column located above the sediments, or re-adsorbed to/co-precipitated with freshly precipitated authigenic FeOx at the iron redox boundary. While the coupling of Fe and P in the marine environment has been recognised as an important component in global biogeochemical cycles, it is often only considered as relevant in the water column or around the zone of dissimilatory Fe reduction (e.g., Slomp et al., 1996a, b; Anschutz et al., 1998; Küster-Heins et al., 2010a, b). However, at continental margins characterised by high accumulation rates of terrigenous siliciclastics, a substantial fraction of FeOx and adsorbed phosphate may escape this shallow Fe redox cycle and get buried into subsurface sediments (e.g., Hensen et al., 2003; Riedinger et al., 2005; März et al., 2008). These FeOx are available for diagenetic processes in deeper parts of the sediment, in particular around the sulphate-methane transition (SMT). At the SMT, a consortium of archaea and bacteria use sulphate to anaerobically oxidize deeper-sourced methane (anaerobic oxidation of methane, AOM; e.g., Hinrichs et al., 1999; Boetius et al., 2000). During AOM, HS^- is generated that reductively dissolves FeOx, leading to the precipitation of Fe sulphides (e.g., greigite, mackinawite, pyrite; Berner, 1970, 1984; Canfield and Berner, 1987; Poulton et al., 2004; Riedinger et al., 2017). During reductive FeOx dissolution, the FeOx-associated phosphate is released to the

ambient pore waters and accumulates as dissolved phosphate at the SMT (e.g., Schulz et al., 1994; Burns, 1997). This phosphate then diffuses out of the SMT into the over- and underlying sediments. Upward-diffusing phosphate will likely re-adsorb onto, or co-precipitate with, detrital or authigenic FeOx above the SMT as long as their surface adsorption capacities are not exhausted (Berner, 1990; Sundby et al., 1992; Slomp et al., 1996a; McManus et al., 1997; Mucci et al., 2000). The phosphate diffusing downwards from the SMT into the methanic zone may precipitate in authigenic form. Detailed insight in the relevant processes is of particular importance for our understanding of the global marine P cycle, as any phosphate buried below the SMT is removed from the oceans over long time scales.

In most marine sediments, authigenic apatite (carbonate fluoroapatite = CFA, also francolite, $Ca_{10}(PO_4, CO_3)_6F_2$) is regarded as the most important long-term P sink (Filippelli, 1997; Delaney, 1998; Ruttenberg, 2003; Canfield et al., 2005). The formation of this mineral has been studied in modern and ancient sedimentary environments (continental shelves, upwelling regions, deep-sea basins; e.g., Sheldon, 1981; Jahnke et al., 1983; Ruttenberg and Berner, 1993; Slomp et al., 1996b; Schuffert et al., 1998; Kim et al., 1999; Schenau et al., 2000; Arning et al., 2008, 2009). However, the formation of Fe(II) phosphates (e.g., vivianite, $Fe(II)_3(PO_4)_2*8(H_2O)$), typical for freshwater systems (e.g., Nriagu, 1972; Mucci et al., 2000; Fagel et al., 2005), has received increasing attention in recent years as evidence of Fe(II) phosphate formation in marine settings is mounting. Formation of vivianite in Chesapeake Bay and Long Island Sound sediments was suggested as early as the 1970s (Bray et al., 1973; Martens et al., 1978; Berner, 1990), mainly based on saturation state calculations from pore water data. Berner (1990) attributed the formation of this marine vivianite to “a rather unusual set of circumstances” including high organic matter input that rapidly consumes sulphate via bacterial sulphate reduction. The lack of sulphate restricts HS^- generation, allowing Fe^{2+} to build up in the pore waters below the sulphate penetration depth. This Fe^{2+} is then available to

react with phosphate released by organic matter degradation to form vivianite. Supporting this hypothesis, recent studies applying sequential extractions and advanced spectroscopic methods (Li et al., 2015; Joshi et al., 2015) identified vivianite (as well as potential Fe(III)-bound P) in anoxic Chesapeake Bay sediments. Applying an unusually wide range of optical, geochemical and mineralogical techniques to sediments of the shallow, brackish Baltic Sea, a close coupling of Fe and P in anoxic sediments below an SMT was recently observed, and the presence of Fe(II) phosphates was unequivocally shown (Jilbert and Slomp, 2013; Slomp et al., 2013; Egger et al., 2015b; Reed et al., 2016; Dijkstra et al., 2016, 2018a, b). Hsu et al. (2014) reported the formation of vivianite below the SMT in South China Sea sediments, including the intergrowth of Fe sulphides with the vivianite micro-aggregates. Even in fully anoxic and sulphidic Black Sea sediments , Fe(II) phosphate formation could play a role for reactive P burial (Dijkstra et al., 2014; Kraal et al., 2017), most likely within sulphate-reducing bacterial cells in AOM consortia (Milucka et al., 2012) and/or below the penetration depth of sulphide (Egger et al., 2016).

All the above settings with tentative or proven vivianite formation are coastal, relatively shallow, marine to brackish environments where organic matter input and burial is high, leading to vigorous early diagenetic processes that favour the formation of authigenic minerals, including Fe(II) phosphates. There are, however, a number of deep, fully marine, relatively organic-poor locations where Fe-P coupling resulting from Fe(II) phosphate formation below the SMT has been identified. On the Amazon Fan (ODP Leg 155; Flood et al., 1995), Burns (1998) reported the occurrence of mm-sized vivianite nodules below the SMT, and attributed their presence to an excess of FeOx over HS^- produced in the SMT. In Zambezi deep-sea fan sediments, März et al. (2008) reported a close Fe-P coupling below the SMT based on pore water and sequential extraction data, which they attributed to Fe(II) phosphate formation, but without identifying discrete Fe(II) phosphate minerals. They also, for the first time, suggested a direct link between the sediment dynamics of the deep-sea fan

system and P diagenesis around the SMT, following an approach developed by Riedinger et al. (2005) for continental margin sediments off the Rio de la Plata.

While studies by Burns (1998) and März et al. (2008) imply vivianite formation in fully marine deep-sea deposits below the SMT, a more systematic understanding of the link between depositional conditions and P diagenesis around the SMT is still lacking. Thus, the aim of this study is to better constrain this understudied part of the P cycle by analysing pore waters, sediments, and P phases around and below the SMT in continental margin sediments off the Zambezi, Amazon, and Rio de la Plata rivers (Fig. 1). We demonstrate that in these settings, coupled cycling of Fe and P occurs within and below the SMT, leading to FeOx dissolution and CFA precipitation within the SMT, and Fe(II) phosphate precipitation below it.

2 Material and Methods

Pore water and sediment samples were collected from gravity cores during several research cruises onboard RV Meteor. Details on the respective cruises, core numbers, locations and lengths as well as water depths are listed in Table 1. Although the cruises took place in different years, the sampling and extraction procedures followed the same protocols, and all sediment analyses were performed on splits of the same sample aliquots. We are therefore certain that results based on material and data from different cruises are consistent and comparable to each other.

Cores were cut into 1 m sections and capped directly after recovery, then stored immediately at 4° C. Within <2 days, the core sections were split, and the working half was immediately transferred into an argon-filled glove box for pore water extraction and sediment sampling. Sediments for pore water extraction were sampled in 25 cm depth resolution. Pore waters

were extracted with a Teflon squeezer setup operated under argon pressure (up to 5 bar) with integrated cellulose acetate filters (0.2 µm pore size) that were stored in oxygen-free distilled water. Sediment samples for sequential Fe and P extractions were taken under anoxic conditions every 10 cm with cut-off plastic syringes, and stored in argon-purged glass bottles at -20° C in darkness.

Pore waters were analysed for total alkalinity, HS^- ($\Sigma H_2S = H_2S + HS^- + S^{2-}$; here defined as HS^-), SO_4^{2-}, PO_4^{3-} and Fe^{2+}, either on the ship or at Bremen University. Continuous sediment sampling for total element analyses was performed in 2 cm depth resolution under oxic conditions. These samples were frozen, freeze-dried, ground in an agate mortar and completely dissolved using a microwave digestion system (conc. HNO_3/HCl/HF mixture). Subsequently, total Fe and P contents were determined by Inductively Coupled Plasma Optical Emission Spectrometry (ICP-OES, Perkin-Elmer Optima 3300RL). More details on pore water and sediment analyses of the studied cores can be found in Kasten et al. (1998), Riedinger et al. (2005), Schulz (2006) and März et al. (2008).

Selected anoxic samples from the four gravity cores were subjected to sequential Fe extractions. For details concerning the selected sample sets and extraction procedures, we refer to Kasten et al. (1998), Hensen et al. (2003) and März et al. (2008). In brief, the operationally defined extractions allowed to determine (1) amorphous and poorly crystalline Fe oxyhydroxides extracted using a buffered ascorbate solution (e.g., ferrihydrite, lepidocrocite; Fe_{asc}), and (2) crystalline Fe oxides using a citrate-buffered dithionite solution (e.g., goethite, hematite; Fe_{dith}) (Ferdelman, 1988; Kostka and Luther, 1994; Haese et al., 2000; Poulton et al., 2004; Haese, 2006).

A sequential phosphate extraction (SEDEX, Ruttenberg, 1992; modified after Schenau and De Lange, 2000) was applied to splits of the same anoxic samples. From each core, one sample above and nine samples within and below the SMT were analysed. The sequential extraction scheme distinguishes between five operationally defined P fractions: Fish bones

(hydroxyapatite) and amorphous apatite precursor phases (e.g., octocalcium-phosphate) (step I, P_{loose}); Fe-bound P (step II, P_{Fe}); authigenic carbonate fluorapatite (step III, P_{CFA}); detrital fluorapatite (step IV, P_{FA}); organic P (step V, P_{org}). The sum of all extraction steps is termed total extracted P (P_{total}). The extraction procedure was performed in an anoxic, argon-flooded glove box, all buffer and extraction solutions were prepared with oxygen-free distilled water, and all extraction vessels were flooded with argon. This was done to prevent a potential bias of P speciation by oxidation of vivianite or iron sulphides (Kraal et al., 2009; Kraal and Slomp, 2014). All P extraction solutions were analysed spectrophotometrically (Skalar Autoanalyser SA 6250 or Perkin-Elmer UV/Vis spectrophotometer 550SE), apart from step 2, which was analysed by ICP-OES (Perkin-Elmer Optima 3300RL).

The aqueous speciation and the saturation indices of selected mineral phases were calculated from the pore water data using the computer programme PHREEQC, which performs a wide variety of aqueous geochemical calculations (Parkhurst and Appelo, 2013). Since the ionic strength of the studied pore waters (0.60 to 0.77 mol/l) is within the range of application for the Debye-Hückel theory, the thermodynamic database ‘phreeqc.dat’ was used in our calculations because it has a relatively wide range of aqueous complexation reactions for twenty-five chemical elements, including P and Fe. It also takes into account the specific volume of ions to derive the pressure dependency of equilibrium constants of aqueous species, and therefore, the pressure dependency of mineral solubility which is an important thermodynamic constraint in deep-sea sediments.

In addition, geochemical inverse models were performed in PHREEQC using data from selected pore water samples in order to test, in terms of the mass-balance of measured dissolved species, the geochemical processes controlling the P and Fe patterns around the SMT. The PHREEQC program calculates sets of mole transfers of phases (minerals, sorbed species) that numerically describe the changes in water chemistry between an initial and a final water composition. These calculations include mole-balance equations for all redox

states of redox-sensitive elements such as Fe, S and C, which are relevant in the SMT. In these models, input data are composed of two analysed pore water compositions, and a selection of geochemical reactions that control the differences between the two compositions. The inverse models developed here are based on a relatively simplified diagenesis and burial history at the study sites, i.e., when sediments are buried, they evolve geochemically from shallow to deeper burial. This geochemical evolution implies that the initial pore water contained in the sediments will react with primary minerals, dissolving them and releasing sorbed species into the pore water, forming secondary minerals, and generating a different pore water composition (i.e., the final pore water in each model). Therefore, two geochemical inverse models were set up for each studied site: Model 1 (within the SMT) describes the changes in pore water chemistry from the sediment-water interface to the SMT. Here, the shallowest sampled pore water and the pore water sampled in the SMT with the highest phosphate content were selected as initial and final waters, respectively. Model 2 (below the SMT) describes the changes in pore water chemistry from the SMT to a point below it. Here, the pore water sampled in the SMT with high phosphate and the pore water sampled below the SMT with low phosphate were selected as initial and final waters, respectively. The pore water samples selected for the inverse models are shown in Table 2. Since authigenic CFA formation demands fluoride pore water data, which are not available for GeoB 9309, we do not include this site in the inverse modelling exercise.

Taking into account the previously described geochemical processes occurring within and below the SMT, and the chemistry of the sampled pore waters, the geochemical processes allowed to occur in the inverse models are: Changes in the redox state of Fe, S, N, C; dissolution of ferrihydrite ($Fe(OH)_3$); precipitation/dissolution of pyrochroite ($Mn(OH)_2$); sorption/desorption of Ca^{2+}, PO_4^{2-}, OH^- and F^- on/from ferrihydrite; precipitation of CFA, vivianite and pyrite; cation exchange of sodium, calcium, and magnesium in clay minerals;

and decomposition of serine ($C_3H_7NO_3$) as a proxy for the biological build-up of ammonium in pore waters.

The input files defined for the geochemical calculations in PHREEQC are based on measured pore water alkalinity, pH, redox potential (Eh), and the aqueous concentration of Na^+, Mg^{2+}, PO_4^{3-}, NO_3^-, NH_4^+, SO_4^{2-}, HS^-, Cl^-, F^-, H_4SiO_4, Mn^{2+} and Fe^{2+}. Since pH and Eh are mandatory input variables for this type of geochemical calculations but were not available for all pore water samples, the average of the values above and below the missing value was assumed. To determine the in situ pressure of each pore water sample at each site, the depth below seafloor, the height of the water column (average sea water density of 1.025 g/cm^3), and the lithostatic pressure (average sediment bulk density of 1.500 g/cm^3) were taken into account. The in situ temperature of each pore water sample was set assuming a temperature of 2.4º C in the shallowest pore water sample, and prescribing a geothermal gradient of 45ºC/km, based on data reported for similar continental margin settings (e.g., Flood et al., 1995). The thermodynamic database used in the PHREEQC calculations as well as the input files for the inverse models can be found in the Supplement.

3 Results

3.1 Pore water data

Geochemical data from all four gravity cores document a pronounced SMT in ~4.5 to ~6.5 m sediment depth, where both sulphate and methane concentrations decrease to below their detection limits, as reported by Kasten et al. (1998), Riedinger et al. (2005), and März et al. (2008). Free HS^- is detected in the pore waters at three of the four studied sites (grey bars in Figs. 2-5).

At all four sites we observe a maximum of pore water phosphate concentrations at the SMT, with up to ~80 µmol/l PO_4^{3-} on the Zambezi fan (GeoB 9309), ~365 µmol/l on the Amazon fan (GeoB 1514), and ~190 µmol/l to ~480 µmol/l off the Rio de La Plata (GeoB 6308 and GeoB 6223, respectively) (Fig. 2). The upward-directed phosphate gradients are almost linear at sites GeoB 6223 and GeoB 6308 between the SMT and the core tops, while phosphate concentrations at sites GeoB 1514 and GeoB 9309 decrease asymptotically and reach values below detection limit in 1-2 m sediment depth. In contrast, the downward-directed phosphate gradients below the SMT are steep at all sites. At sites GeoB 1514 and GeoB 9309, phosphate is completely removed from the pore waters within one meter or less below the SMT, while in cores GeoB 6223 and GeoB 6308 phosphate declines to 50-100 µmol/l.

Dissolved Fe^{2+} concentrations (Fig. 2) show a strong relationship to the SMT and the availability of free sulphide at the four study sites. While no Fe^{2+} is detectable within the sulphidic zone around the SMT, its concentrations generally increase above and below this zone, despite some scatter in the data. While maximum Fe^{2+} concentrations below the SMT reach ~100 µmol/l in the sediments at Site GeoB 1514, they are ~18 µmol/l in core GeoB 6223, ~10 µmol/l in core GeoB 9309, and ~2 µmol/l in core GeoB 6308. Elevated Fe^{2+} concentrations above the SMT are only observed at sites GeoB 1514 (up to 50 µmol/l in ~400-100 cm depth) and GeoB 9309 (up to 12 µmol/l in ~250-100 cm depth).

Pore water concentrations of Ca^{2+} and F^- (Fig. 3) display different patterns across the SMT in the studied sediments. While Ca^{2+} at sites GeoB 6223 and 6308 follows a linear trend from the sediment surface to the SMT where it is partially consumed, the Ca^{2+} profiles at sites GeoB 1504 and 9309 cross the SMT without any obvious changes. The F^- profiles show minima in the SMT at sites GeoB 1504, 6223 and 6308, while no F^- data are available for core GeoB 9309.

All pore water and sediment data are available from the data archive PANGAEA operated by the World Data Centers for Marine Environmental Sciences (http://www.pangaea.de/PangaVista).

3.2 Solid phase data

The results of sequential FeOx extractions show minimum contents of amorphous and crystalline Fe (oxyhydr)oxides (sum of Fe_{asc} and Fe_{dith} fractions) at the SMT (Fig. 2). Below the SMT, FeOx contents are equal to, or higher than, FeOx above the SMT (Fig. 2). Amongst the two extracted FeOx pools, Fe_{asc} contents are <20 µmol/g within the SMT, while Fe_{dith} values are below 100 µmol/g (Fig. 4; no data for core GeoB1514). These values correspond to <3 relative percent (rel%) and <10 rel% of total sedimentary Fe, respectively. Above the SMT, Fe_{dith} is higher than Fe_{asc}, while the opposite is true below the SMT (Fig. 4). In detail, the Fe_{asc} contents directly below the SMT increase to ~70 µmol/g (8-10 rel% of total Fe) at sites GeoB 9309 and GeoB 6223, and to ~40 µmol/g (6 rel% of total Fe) at site GeoB 6308 (Fig. 4).

The P fractions extracted in each of the five extraction steps are displayed in Figure 5 (in µmol/g of dry sediment) and Figure 6 (as rel% of P_{total}). There are significant similarities in P speciation at all sites. The P_{loose} fraction is relatively minor at all sites, displaying highest contents as well as relative percentages to total P close to the sediment surface (<4 µmol/g, <22 rel% of P_{total}), and lowest contents below the SMT (<1 µmol/g, <4 rel% of P_{total}). At sites 6308 and 9309, P_{loose} is also higher (~15-17 rel%) within the SMT (Fig. 6).

The Fe-bound P (P_{Fe}) fraction is dominant at all sites but GeoB 6308 (Figs. 5, 6). It constitutes on average 41 rel% of P_{total} in core GeoB 9309, 33 rel% in core GeoB 6223, 46 rel% in core GeoB 1514, and 17 rel% in core GeoB 6308. At the three former sites, the P_{Fe} fraction is

lowest within the SMT, accounting for 25 rel% in core GeoB 9309, 30 rel% in core GeoB 6223, and 42 rel% in core GeoB 1514 of P_{total}. In contrast, the P_{Fe} fraction tends to increase below the SMT (on average 54 rel% in core GeoB 9309, 38 rel% in core GeoB 6223, 49 rel% in core GeoB 1514 of P_{total}).

Authigenic carbonate fluorapatite (P_{CFA}) is a significant fraction in sediments off the Rio de la Plata (on average 29 rel% and 42 rel% of P_{total} in cores GeoB 6223 and GeoB 6308, respectively), but less important at the Amazon and Zambezi deep-sea fan sites (on average 16 rel% and 11 rel% of P_{total}, respectively). In contrast to the P_{Fe} fraction, P_{CFA} exhibits maxima within the SMT at all sites (Fig. 6).

In contrast to authigenic carbonate fluorapatite, detrital fluorapatite (P_{FA}) is quantitatively more important at the Amazon and Zambezi sites (on average 24 rel% and 18 rel% of P_{total}, respectively) than off the Rio de la Plata (on average 13 rel% and 14 rel% of P_{total}, respectively). At all sites, P_{FA} exhibits highest absolute and relative contents below the SMT (Figs. 5, 6). This fraction will not be discussed any further in this study, as detrital fluorapatite is the most stable P mineral in marine sediments and unlikely to participate in early diagenetic dissolution-precipitation reactions on the time scales discussed here.

Organic P (P_{org}) is a minor P fraction at all four sites, ranging from 5 rel% off the Rio de la Plata to 13 rel% off the Amazon, typically with highest relative contributions near the sediment surface (Fig. 6).

3.3 PHREEQC results

The aqueous speciation calculations performed in PHREEQC reveal that at all sites the saturation index (SI) for hydroxyapatite is highest within the SMT, consistently reaching oversaturation (Fig. 7). Above and below the SMT, the hydroxyapatite SI decreases and the

pore waters become undersaturated at the top and bottom of each sediment column, except for GeoB 6223 where the pore waters are oversaturated throughout the sediment column (Fig. 7). The vivianite SI indicates that at GeoB 6308 and 9309, the pore waters are undersaturated with respect to vivianite throughout the sediment column but, despite some scatter, there are slight increases of the SI below the SMT. This is also observed at GeoB 6223 where saturation is reached in two samples below the SMT. At GeoB 1514, the pore waters become saturated with respect to vivianite below 100 cm depth down to the bottom of the core, and oversaturated in two samples below the SMT (Fig. 7).

The results of the geochemical inverse models performed in PHREEQC based on mass-balance of chemical species, pH and redox potential of the sampled pore waters, are shown in Figure 8 and Table 3). In Model 1, the changes in water chemistry between the sediment-water interface and the SMT are explained by the dissolution of ferrihydrite, desorption of P from ferrihydrite, predominant precipitation of CFA, and minor precipitation of vivianite, pyrite and pyrochroite at the three sites (1514, 6223, 6308). In Model 2, the changes in composition from pore waters within to below the SMT are explained by the dissolution of ferrihydrite, desorption of P from ferrihydrite, and predominant precipitation of vivianite at Sites 1514 and 6308, while at Site 6223 precipitation of CFA is predominant.

4 Discussion

4.1 Re-adsorption of P onto Fe (oxyhydr)oxides below the SMT

Results of sequential iron extractions performed by Kasten et al. (1998), Hensen et al. (2003), Riedinger et al. (2005, 2014), and März et al. (2008) showed that in continental slope sediments off the Amazon, Rio de La Plata and Zambezi rivers, significant amounts of FeOx

are preserved in methanic sediments below the SMT. The amorphous to crystalline minerals included in this FeOx pool (e.g., ferrihydrite, goethite, hematite, magnetite) are highly reactive with respect to HS^- (Poulton et al., 2004). Under sulphidic conditions similar to those prevailing at an SMT, these FeOx phases have approximate half-lives of 12 hours to ~1 year, as experimentally determined by Poulton et al. (2004) (sea water, pH 7.5, 25°C). The observed preservation of these FeOx in marine sediments deposited thousands of years ago was most likely caused by the rapid migration of the SMT under high sedimentation rates (~80-100 cm/kyr off the Zambezi and Rio de la Plata) prior to the Holocene sea level rise (Riedinger et al., 2005; März et al., 2008; Schefuβ et al., 2011; Van der Lubbe et al., 2014). The resulting relatively short exposure of FeOx minerals to sulphidic conditions in the SMT led to incomplete FeOx reduction and sulphidisation, and ultimately to the burial of FeOx in sediments below the SMT (e.g., Riedinger et al., 2005; 2014). Phosphate diffusing downward out of the current SMT could re-adsorb onto these buried FeOx minerals, a process that is predicted in the geochemical inverse Model 2 for Site 6223 (Table 3). This, however, would not explain the much steeper pore water phosphate gradient below the SMT compared to the gradient above. The phosphate adsorption capacity of FeOx is a function of their surface area, which decreases during progressive burial and aging of FeOx (Lijklema, 1980; Crisby et al., 1981; Wang et al., 2013). Therefore, the adsorption capacity of FeOx above the SMT should be higher than that of aged FeOx buried below the SMT. The results of the geochemical inverse models reflect this tendency, i.e., higher relative amounts of P bound to ferrihydrite in shallow pore waters (i.e., the initial waters of Model 1, in Table 3) than in the deeper pore waters (the remaining pore waters in Table 3). In contrast, pore water profiles indicate a more rapid removal of phosphate below than above the SMT, and re-adsorption onto FeOx alone cannot be responsible for this pattern, as shown in the results of the geochemical inverse models (Table 3). While we cannot exclude re-adsorption of phosphate onto FeOx surfaces

below the SMT, the data point towards precipitation of an authigenic phosphate mineral, which will be discussed in the following.

4.2 Authigenic mineral precipitation - carbonate fluorapatite (CFA) or hydroxyapatite

While authigenic CFA in marine sediments has been studied for decades, the exact formation mechanism is still not fully understood. It appears to proceed via either poorly crystalline, Ca-rich precursor phases or hydroxyapatite (Van Cappellen and Berner, 1988, 1991; Schenau et al., 2000; Gunnars et al., 2004; Omelon and Grynpas, 2008; Oxmann and Schwendenmann, 2014), although polyphosphate storage by phytoplankton or giant sulphur bacteria has been suggested as an alternative pathway (Schulz and Schulz, 2005; Diaz et al., 2008; Arning et al., 2009). A common observation in marine sediments is an increase of CFA with burial depth, likely due to the transfer of P from more labile forms into CFA ("sink switching"; e.g., Ruttenberg and Berner, 1993; Delaney, 1998; Anderson et al., 2001). Sink switching is considered to be the dominant process of CFA authigenesis in ocean sediments worldwide, leading to the long-term burial of P in marine deposits (e.g., Froelich et al., 1982; Ruttenberg and Berner, 1993; Filippelli, 2008). In addition, CFA precipitation has recently been suggested to occur in Black Sea sediments following phosphate release at the SMT and its upward diffusion (Egger et al., 2016).

In the studied sediment cores, CFA makes up a significant portion of the total P pool, supporting its overall importance in marine P burial. However, neither amorphous CFA precursor phases (including hydroxyapatite, extracted during step I) nor CFA (extracted during step III) were found to be systematically higher below the SMT than above it at any of the study sites. Thus, CFA formation does not appear to be the dominant sink for pore water phosphate below the SMT in any of the sediment cores, despite appreciable concentrations of

both phosphate and calcium in the pore water. This could be related to the lack of calcium carbonate surfaces as nuclei for CFA precipitation (deKanel and Morse, 1978), making these carbonate-poor deposits unfavourable for significant CFA formation despite high pore water phosphate build-up. We conclude that CFA authigenesis is not responsible for the distinct decrease in pore water phosphate below the SMT at any of the four study sites. This is supported by PHREEQC calculations, revealing that the SI of hydroxyapatite decreases below the SMT at all sites, and reaches undersaturation at three of four sites. In addition, the results of the geochemical inverse models also indicate that CFA formation below the SMT at sites 1514 and 6308 is negligible (Model 2, Table 3).

In contrast, samples within the SMT show high absolute and relative CFA contents at all four sites (Figs. 5, 6). We suggest that the steady supply of pore water phosphate from dissolving FeOx minerals creates geochemical conditions favourable for the precipitation of authigenic apatite. Indeed, at sites GeoB 6308 and GeoB 9309, P_{loose} is highest at the SMT (Figs. 5, 6), and this fraction should include – in addition to some pore water phosphate – amorphous CFA precursor phases. The higher saturation indexes for hydroxyapatite obtained in PHREEQC calculations generally suggest favourable thermodynamic conditions for the formation of authigenic hydroxyapatite within the SMT at all studied sites, possibly as a precursor phase of CFA (Fig. 7). In addition, in terms of mass-balance of the observed pore water chemistry, the geochemical inverse Model 1 predicts significant CFA formation in the SMT at the three modelled sites (Fig. 8 and Table 3).

Regarding Ca and F uptake into CFA or its precursor phases, the pore water profiles of Ca^{2+} and F^- are ambivalent at the different sites (Fig. 3). These differences in Ca^{2+} and F^- profiles could be related to the formation of authigenic carbonates known to precipitate at the SMT in continental margin sediments (Meister et al., 2007; Pierre et al., 2016; Wehrmann et al., 2016), and concurrent formation of CFA and authigenic carbonates might occur at some of our study sites. At site GeoB 6223, the SMT acts as a sink for pore water Ca^{2+} and F^-,

indicating CFA formation in support of P extraction data (Figs. 5, 6). At site GeoB 1514, there is a modest pore water F^- gradient into the SMT, but Ca^{2+} appears to be unaffected. At site GeoB 6308, Ca^{2+} and F^- show a pronounced parallel minimum, but it is located ~1 m above the phosphate peak and is concurring with high P_{loose} instead of CFA contents (Figs. 5, 6). At site GeoB 9309, the P extraction data suggest formation of CFA and its precursors, but the SMT does not appear to act as a significant sink of pore water Ca^{2+}, and no F^- data are available for this site. Overall, our data and the results of the geochemical inverse models indicate that SMTs in continental margin sediments act as zones of CFA formation, but there are significant differences between study sites. We can, however, clearly state that CFA or hydroxyapatite formation as the predominant phosphate sink below the SMT is neither supported by solid phase nor by pore water data and PHREEQC calculations.

4.3 Authigenic mineral precipitation - Fe(II) phosphates

As discussed in the Introduction, the formation of Fe(II) phosphates like vivianite represents one of the dominant burial forms of P in lacustrine and estuarine sediments (e.g., Nriagu, 1972; Nembrini et al., 1983; Mucci et al., 2000; Fagel et al., 2005; Cosmidis et al., 2014). It has also been reported in some brackish to marine settings (Nriagu, 1972; Bray et al., 1973; Martens et al.1978; Burns, 1997; März et al., 2008; Dellwig et al., 2010; Taldenkova et al., 2010; Jilbert and Slomp, 2013; Slomp et al., 2013; Hsu et al., 2014; Dijkstra et al., 2014; Li et al., 2015; Egger et al., 2015b; Reed et al., 2016; Dijkstra et al., 2016, 2018a, b). Based on solid phase and pore water data presented in this study, there is a strong geochemical argument for the formation of Fe(II) phosphates in the methanic zone below the SMT in continental margin sediments off the Zambezi, Rio de la Plata and Amazon rivers. While dissolved phosphate is released within the SMT, the source of dissolved iron below the SMT is more ambiguous. As suggested by Beal et al. (2009), iron reduction in methanic (non-

sulphidic) marine sediments could potentially be coupled to the anaerobic oxidation of methane. This process has recently been proposed for the Argentine margin off the Rio de la Plata (Riedinger et al., 2014), the Baltic Sea (Egger et al., 2015a, 2017), and the North Sea (Oni et al., 2015). Alternatively, Sivan et al. (2016) suggested that high Fe^{2+} concentrations in pore waters of methanic sediments could result from a rapid switch between methanogenesis and dissimilatory iron reduction. While the exact nature of iron-methane coupling in anoxic/methanic marine sediments is debated, we suggest that the unambiguous presence of Fe^{2+} below the SMT-associated sulphidic zone is important for the P cycle.

As stated above, our data provide evidence of a tight coupling of Fe and P below the SMT in the studied sediments, and suggest that this coupling is due to the precipitation of Fe(II) phosphate minerals. The SI of vivianite (Fig. 7) indicates that at GeoB 1514 this mineral is likely forming below 100 cm depth and especially below the SMT. At the other sites, despite vivianite unsaturation, the relative increase of the calculated SI indicates that this mineral is more likely to form below the SMT. In addition, vivianite precipitation in this type of sediments is most likely controlled by relatively slow reaction kinetics (which are not taken into account by PHREEQC calculations when calculating aqueous speciation and the corresponding SI). Hence, we suggest that vivianite may form even where the SI indicates unsaturated pore water conditions. This hypothesis is corroborated by the results of the geochemical inverse Model 2 for the three modelled sites where vivianite is predicted to form below the SMT.

In contrast to past studies in lacustrine, brackish or marine sediments (e.g., Burns, 1997; Fagel et al., 2005; Dijkstra et al., 2016), we were not able to identify vivianite macroscopically, microscopically, or mineralogically (by XRD) in any of the studied sediment samples below the SMT. While vivianite forms micronodules in Amazon Fan sediments studied by Burns (1997) and in Baltic Sea deposits (e.g., Egger et al., 2015b; Dijkstra et al., 2016, 2018a, b), no such aggregates are present in any of the continental margin sediments studied here. Instead,

Fe(II) phosphates seem to be finely dispersed in the sediment, and are thus not detectable using any of the above techniques. This is supported by the results obtained in the geochemical inverse Model 2 (Fig. 8) where the amount of vivianite predicted to form below the SMT in the three modelled sites is below 0.07 wt%. This issue has been pointed out in the past, and has mainly been related to low contents, and very fast oxidation of Fe(II) phosphates in marine sediments upon recovery (Nriagu, 1972; Nembrini et al., 1983; Pratesi et al., 2003; Fagel et al., 2005). Our approach of applying sequential extraction schemes to distinguish Fe(II) phosphates from other sedimentary Fe and P fractions, especially in combination with PHREEQC calculations, is promising and has been successfully applied in the Baltic Sea (e.g., Egger et al., 2015b; Dijkstra et al., 2016, 2018a, b). However, information about the selectivity of specific extraction steps for Fe(II) phosphates (or their oxidation products) is still limited. Nembrini et al. (1983) studied freeze-dried sediments (stored in a desiccator) from Lago Maggiore using Mössbauer spectroscopy, and identified vivianite with the structural Fe partly or fully oxidised. Subsequently, they showed that most of the Fe-bound P was extracted by a citrate-buffered dithionite (CDB) solution. In the study presented here, we applied P extraction (Ruttenberg, 1992; Schenau et al., 2000; Schenau and De Lange, 2000) and Fe extraction schemes (Ferdelman, 1988) where the Fe-bound P and the FeOx fractions are extracted with the same solution that Nembrini et al. (1983) used to extract vivianite. Dijkstra et al. (2014) showed that almost 100% of vivianite (synthesized, freeze-dried and extracted under strictly anoxic conditions) was dissolved by sequential hydroxylamine-HCl (HH) and CDB extractions. We hence conclude that the extraction steps used in this study to leach Fe-bound P and FeOx from deep-sea fan sediments (under anoxic sampling, storage, and extraction conditions) have also extracted Fe(II) phosphates from the samples, supporting our argument of vivianite formation at the four study sites below the SMT.

4.4 Global relevance of Fe(II) phosphate formation in continental margin and deep-sea fan sediments

Our study shows that formation of Fe(II) phosphates in marine sediments can occur under the following conditions: the absence of sulphate and hydrogen sulphide, presence of dissolved Fe and P in the pore waters, and a depositional mechanism to bury significant amounts of FeOx below the SMT. These conditions are met in a variety of depositional settings, and one prominent example that has been studied in detail over the last years is the Baltic Sea. In the episodically sulphidic Landsort Deep, lacustrine FeOx-rich deposits are overlain by organic-rich brackish sediments, allowing vivianite nodules to grow at the boundary between these sediment units as dissolved phosphate and iron are delivered from above and below, respectively (Dijkstra et al., 2016). Similar processes are responsible for vivianite formation in the Bothnian Sea (Slomp et al., 2013; Egger et al., 2015b Dijkstra et al., 2018a), but at much shallower sediment depths. A critical aspect at all of these sites, as well as in Zambezi Fan sediments studied by März et al. (2008), is the presence of an SMT and an FeOx pool buried beneath it that is gradually reduced (Egger et al., 2015a, 2016).

While many of these conditions are typically met along continental margin settings, our study indicates that for a significant Fe(II) phosphate enrichment at a specific sediment depth, the SMT and associated diagenetic processes need to occur within the same sediment layer for a prolonged period of time (thousands of years). The fixation of an SMT within a distinct sediment horizon, but also the preservation of significant amounts of reactive FeOx beneath it, require a particular sedimentation regime: Rapid, mostly terrigenous sedimentation followed by long-lasting, much lower sedimentation rates that allow a new stable diagenetic regime to develop. As shown by Kasten et al. (1998), Riedinger et al. (2005, 2014) and März et al. (2008), these conditions are met on deep-sea fans/depocenters off large rivers. Especially around the last deglaciation, sedimentation rates on many deep-sea fans and continental slope

depocenters worldwide (including those off the Amazon, Zambezi and Rio de la Plata rivers) dramatically dropped due to the trapping of riverine sediment on the flooded continental shelves (Shanmugan et al., 1985; Covault and Graham, 2010) (Fig. 9). The transitional part of the deglaciation, i.e., when new accommodation space became available on the shelf and the delivery of sediment to the continental slope was switched off, was rather short and is not expected to have left a record in pore water or sediment geochemistry. Subsequently, low sedimentation rates prevailed at the deep sea depo-enters over several thousands of years. Notably, other sediment cores from the Rio de La Plata margin show some deviations in the depth of the present-day SMT and the thickness of the sulfidic zone (Henkel et al., 2011, 2012). This heterogeneity is related to the very dynamic sedimentation processes especially at continental margins with high sediment accumulation rates, recurrent mass wasting, shifting channel-levee systems, and/or changes in methane flux from below (some of which also affected the Zambezi depocenter; Wiles et al., 2017). In addition, not all deep-sea fans or continental slope depocenters experienced the same drastic decrease in sedimentation rates during the last deglacial sea level rise. Indeed, some deep-sea fan systems have continually accumulated sediment over the last 35,000 years (Covault and Graham, 2010), preventing the establishment of non-steady state diagenetic conditions and the fixation of the SMT at a certain sediment depth. These fan systems were usually either (a) adjacent to narrow continental shelves that did not provide sufficient new accommodation space to trap most of the riverine sediment load, or (b) located in areas where freshwater input (and thus riverine sediment input) strongly increased after the last deglaciation (e.g., glacial melt water, monsoonal rainfall). Thus, the sequence of initially high, then much lower sedimentation rates across the last deglaciation only occurred on deep-sea fans and slope depocenters that are adjacent to a wide shelf on a passive continental margin, and that did not experience systematic increases in riverine sediment input.

We combine the compilation of Covault and Graham (2010) of true deep-sea fans where sedimentation rates dropped following the last deglaciation with size estimates of the fans (Barnes and Normark, 1985) to put the importance of sub-SMT vivianite formation into a global context. With the Amazon fan (~330,000 km^2) and the Nitinat fan (~23,000 km^2) alone, the potential loci for sub-SMT vivianite formation on continental margins cover an area about as large as the Baltic Sea. Realistically, the conditions for sub-SMT vivianite formation are given along vast stretches of low to mid-latitude passive continental margins where the spatial extents of the fine-grained, riverine sediment depocenters (that are often not true submarine fans) are poorly quantified (e.g., off the Zambezi and Rio de la Plata). This applies in particular to the passive continental margins of North and South America, Asia, Africa and Europe bordered by wide continental shelves, unaffected by uplifting mountains or an ice sheet in the hinterland, and supplied with sediment by major rivers. Our data also show that sub-SMT vivianite formation can occur in water depths of ~1,200 m (Zambezi) to ~4,200 m (Rio de la Plata), depending on the geometry and sedimentation pattern of the specific continental margin. We hence propose that the sub-SMT formation of vivianite in continental margin sediments is of global importance for the marine P budget.

5 Conclusion

Our compilation of geochemical data from three deep-sea fan systems off the Zambezi, Amazon and Rio de la Plata river mouths provides new insights into the dynamics of P cycling in marine sediments affected by anaerobic oxidation of methane and deep iron reduction within the methanic zone. While CFA appears to be an important sink for P directly within the SMT, we find that in the studied sediments the formation of CFA below the SMT is not the dominant sink for pore water phosphate. Pore water and sediment analyses reveal

that the geochemical conditions found below the SMT at the four studied locations are favourable for the formation of Fe(II) phosphate minerals like vivianite. The required geochemical pre-conditions for Fe(II) phosphate formation in general are: (a) Dominantly terrigenous sediment input to provide sufficient reactive FeOx as phosphate adsorption sites; (b) high sedimentation rates to quickly bury FeOx and associated phosphate into the sediments; (c) low rates of reactive organic matter accumulation to preserve FeOx below the zone of dissimilatory Fe reduction; (d) reactive FeOx within the SMT to limit HS^- to a thin sulphidic zone; (e) dissolution of FeOx within the sulphidic zone to release phosphate into the pore waters; (f) the lack of biogenic carbonate surfaces to act as nuclei for CFA precipitation; and (g) the diagenetic release of Fe^{2+} into the pore waters below the SMT. In addition, our study shows that, to allow for the development of significant authigenic Fe(II) phosphate mineral enrichments below the SMT, this diagenetic zone needs to be fixed at a specific sediment interval for thousands of years, for example in response to glacial-interglacial sea level changes.

These conditions are met in deep-sea fan and continental slope depositional systems adjacent to wide shallow shelf areas that experienced a sudden shift from high to low sedimentation rates (Fig. 9). Our results therefore add to the mounting evidence that authigenesis of Fe(II) phosphates is wide-spread in marine systems and constitutes a currently underestimated P sink in the ocean. The estimation of any Fe(II) phosphate budgets for the marine environment as a whole is still compromised by poor data coverage, in particular when it comes to the quantification of Fe(II) phosphates in settings where these phases do not occur as readily identifiable micronodules. Our study, however, offers a systematic attempt to understand Fe(II) phosphate formation in the marine environment that may assist in identifying depositional settings where these minerals are likely to form, and to assess the relevance of authigenic Fe(II) phosphates for global marine P and Fe cycling. Promising analytical approaches are offered by combining standard pore water and sediment analysis with cutting-

edge spectroscopic and microanalytical techniques (as applied, e.g., by Jilbert and Slomp; Dijkstra et al., 2014; Egger et al., 2015; Li et al., 2015) and modified, more selective sequential extraction schemes (Gu et al., 2016).

6 Acknowledgements

The authors thank masters, crews, and scientists onboard RV Meteor cruises M16/2, M46/2, M46/3 and M63/1 for assistance with taking the gravity cores. Analytical support by Jan Hoffmann, Silvana Pape, Karsten Enneking and Martin Kölling, either on board or at Bremen University, is gratefully acknowledged. Special thanks go to Laurel Childress for generating the maps in Figure 1, and to David Parkhurst for his valuable comments on the PHREEQC models. This study benefitted from discussions with Christoph Vogt, Horst Schulz, Caroline Slomp, Matthias Egger, Peter Kraal, Katrin Küster-Heins, Gert de Lange, and from insightful reviews by Gabriel Filippelli, an anonymous reviewer, and editor Gert de Lange. This study was partly funded by the DFG Graduate College EUROPROX (CM).

Literature

Anderson, L.D., Delaney, M.L., Faul, K.L., 2001. Carbon to phosphorus ratios in sediments: implications for nutrient cycling. Global Biogeochem. Cycles 15, 65-79.

Anschutz, P., Zhong, S., Sundby, B., Mucci, A., Gobeil, C., 1998. Burial efficiency of phosphorus and the geochemistry of iron in continental margin sediments. Limnol. Oceanogr. 43, 53-64.

Arning, E.T., Lückge, A., Breuer, C., Gussone, N., Birgel, D., Peckmann, J., 2008. Genesis of phosphorite crusts off Peru. Mar. Geol. 262, 68-81.

Arning, E.T., Birgel, D., Brunner, B., Peckmann, J., 2009. Bacterial formation of phosphatic laminites off Peru. Geobiol. 7, 295-307, doi:10.1111/k.472-4667.2009.00197.x.

Barnes, N.E., Normark, W.R., 1985. Diagnostic parameters for comparing modern submarine fans and ancient turbidite systems. In: Bouma, A.H., Normark, W.R., Barnes, N.E. (Eds.), Submarine Fans and Related Turbidite Systems, Springer-Verlag, New York, 13-14.

Beal, E.J., House, C.H., Orphan, V.J., 2009. Manganese- and iron-dependent marine methane oxidation. Science 325, 184-187.

Berner, R.A., 1970. Sedimentary pyrite formation. Am. J. Sci. 268, 1–23.

Berner, R.A., 1973. Phosphate removal from sea water by adsorption on volcanogenic ferric oxides. Earth Planet. Sci. Lett. 18, 77–86.

Berner, R.A., 1984. Sedimentary pyrite formation: an update. Geochim. Cosmochim. Acta 48, 605–615.

Berner, R.A., 1990. Diagenesis of phosphorus in sediments from non-upwelling areas. In: Burnett, W.C., Riggs, S.R. (Eds.), Phosphate Deposits of the World Volume 3: Neogene to Modern Phosphorites. Cambridge University Press, 27-32.

Boetius, A., Ravenschlag, K., Schubert, C.J., Rickert, D.,Widdel, F., Gieseke, A., Amann, R., Jørgensen, B.B., Witte, U., Pfannkuche, O., 2000. A marine microbial consortium apparently mediating anaerobic oxidation of methane. Nature 407, 623–626.

Bray, J.T., Bricker, O.P., Troup, B.N., 1973. Phosphate in interstitial waters of anoxic sediments: oxidation effects during sampling procedure. Science 180, 1362-1364.

Burns, S.J., 1997. Early diagenesis in Amazon Fan sediments. In: Flood, R.D., Piper, D.J.W., Klaus, A., Peterson, L.C. (Eds.), Proc. ODP Sci. Results, vol. 155. (Ocean Drilling Program), College Station, TX, pp. 497–504.

Canfield, D.E., Berner, R.A., 1987. Dissolution and pyritization of magnetite in anoxic marine sediments. Geochim. Cosmochim. Acta 51, 645–659.

Canfield, D.E., Kristensen, E., Thamdrup, B., 2005. The phosphorus cycle. In: Canfield, D. E., Kristensen, E., Thamdrup, B. (Eds.), Aquatic Geomicrobiology. Advances in Marine Biology, vol. 48, pp. 419–440.

Cosmidis, J., Benzerara, K., Morin, G., Busigny, V., Lebeau, O., Jézéquel, D., Noël, V., Dublet, G., Othmane, G., 2014. Biomineralization of iron-phosphates in the water column of Lake Pavin (Massif Central, France). Geochim. Cosmochim. Acta 126, 78–96.

Covault, J.A., Graham, S.A., 2010. Submarine fans at all sea-level stands: tectono-morphologic and climatic controls on terrigenous sediment delivery to the deep sea. Geology 38, 939-942.

Crosby, S.A., Butler, E.I., Turner, D.R., Whitfield, M., Glasson, D.R., Millward, G.E., 1981. Phosphate adsorption onto iron oxyhydroxides at natural concentrations. Environ. Technol. Lett. 2, 371-378.

DeKanel, J., Morse, J.W., 1978. The chemistry of orthophosphate uptake from seawater onto calcite and aragonite. Geochim. Cosmochim. Acta 42, 1335–1340.

Dellwig, O, Leipe, T, März, C., Glockzin, M., Pollehne, F., Schnetger, B., Yakushev, E.V., Boettcher, M.E., Brumsack, H-J., 2010. A new particulate Mn–Fe–P-shuttle at the redoxcline of anoxic basins. Geochim. Cosmochim. Acta 74, 7100–7115.

Delaney, M.L., 1998. Phosphorus accumulation in marine sediments and the oceanic phosphorus cycle. Glob. Biogeochem. Cycles 12, 563–572.

Diaz, J.M., Ingall, E.D., Benitez-Nelson, C., Paterson, D., de Jonge, M., McNulty, I., Brandes, J.A., 2008. Marine polyphosphate: A key player in geologic phosphorus sequestration. Science 320, 652–655.

Dijkstra, N., Kraal, P., Kuypers, M.M.M., Schnetger, B., Slomp, C.P., 2014. Are iron-phosphate minerals a sink for phosphorus in anoxic Black Sea sediments? PLoS ONE 9(7), e101139. doi:10.1371/journal.pone.0101139.

Dijkstra, N., Slomp, C.P., Behrends, T., Expedition 347 Scientists (2016) Vivianite is a key sink for phosphorus in sediments of the Landsort Deep, an intermittently anoxic deep basin in the Baltic Sea. Chem. Geol. 438, 58-72.

Dijkstra, N., Quintana Krupinski, N.B., Yamane, M., Obrochta, S.P., Miyairi, Y., Yokoyama, Y., Slomp, C.P. (2018a) Holocene refreshening and reoxygenation of a Bothnian Sea estuary led to enhanced phosphorus burial. Est. Coasts, 41, 139-157.

Dijkstra, N., Hagens, M., Egger, M., Slomp, C.P. (2018b) Post-depositional formation of vivianite-type minerals alters sediment phosphorus records. Biogeosci. 15, 861-883.

Egger, M., Rasigraf, O., Sapart, C.J., Jilbert, T., Jetten, M.S.M., Röckmann, T., Van der Veen, C., Bândă, N., Kartal, B., Ettwig, K.F., Slomp, C.P., 2015a. Iron-mediated anaerobic oxidation of methane in brackish coastal sediments. Environ. Sci. Technol. 49, 277-283.

Egger, M., Jilbert, T., Behrends, T., Rivard, C., Slomp, C.P., 2015b. Vivianite is a major sink for phosphorus in methanogenic coastal surface sediments. Geochim. Cosmochim. Acta 169, 217-235.

Egger, M., Kraal, P., Jilbert, T., Sulu-Gambarini, F., Sapart, C.J., Röckmann, T., Slomp, C.P., 2016. Anaerobic oxidation of methane alters sediment records of sulfur, iron and phosphorus in the Black Sea. Biogeosci. 13, 5333-5355.

Egger, M., Hagens, M., Sapart, C.J., Dijkstra, N., van Helmond, N.A.G.M., Mogollón, J., Risgaard-Petersen, N., Van Der Veen, C., Kasten, S., Riedinger, N., Böttcher, M.E., Röckmann, T., Jørgensen, B.B., Slomp, C.P., 2017. Iron oxide reduction in methane-rich deep Baltic Sea sediments, Geochim. Cosmochim. Acta 207, 256–276.

Einsele, W., 1938. Über chemische und kolloidchemische Vorgänge in Eisenphosphat-Systemen unter limnochemischen und limnogeologischen Gesichtspunkten. Arch. Hydrobiol. 33, 361–387.

Fagel, N., Alleman, L.Y., Granina, L., Hatert, F., Thamo-Boszo, E., Cloots, R., André, L., 2005. Vivianite formation and distribution in Lake Baikal sediments. Glob. Planet. Change 46, 315–336.

Feely, R.A., Trefry, J.H., Massoth, G.J., Metz, S., 1991. A comparison of the scavenging of phosphorus and arsenic from seawater by hydrothermal iron oxyhydroxides in the Atlantic and Pacific Oceans. Deep-Sea Res. 38, 617-623.

Ferdelman, T.G., 1988. The distribution of sulfur, iron, manganese, copper,and uranium in a salt marsh sediment core as determined by a sequential extraction method. Masters thesis, Univ. Delaware.

Filippelli, G.M., 1997. Controls on phosphorus concentrations and accumulation in oceanic sediments. Mar. Geol. 139, 231–240.

Filippelli, G.M., 2008. The global phosphorus cycle: past, present, and future. Elements 4, 89-95.

Flood, R.D., Piper, D.J.W., Klaus, A., et al., 1995. Proc. ODP, Init. Repts., 155: College Station, TX (Ocean Drilling Program).

Froelich, P.N., Klinkhammer, G.P., Bender, M.L., Luedtke, N.A., Heath, G.R., Cullen, D., Dauphin, P., Hammond, D., Hartman, B., Maynard, V., 1979. Early oxidation of organic matter in pelagic sediments of the eastern equatorial Atlantic: suboxic diagenesis. Geochim. Cosmochim. Acta 43, 1075-1090.

Froelich, P.N., Bender, M.L., Luedtke, N.A., Heath, G.R., DeVries, T., 1982. The marine phosphorus cycle. Am. J. Sci. 282, 474-511.

Goldberg, E.D., 1954. Marine geochemistry. 1. Chemical scavengers of the sea. J. Geol. 62, 249-265.

Gu, S., Qian, Y., Jioa, Y., Li, Q., Pinay, G., Gruau, G., 2016. An innovative approach for sequential extraction of phosphorus in sediments: Ferrous iron P as an independent P fraction. Water Res. 103, 352-361.

Gunnars, A., Blomqvist, S., Martinsson, C., 2004. Inorganic formation of apatite in brackish seawater from the Baltic Sea: an experimental approach. Mar. Chen. 91, 15-26.

Haese, R.R., Schramm, J., Rutgers van der Loeff, M.M., Schulz, H.D., 2000. A comparative study of iron and manganese diagenesis in continental slope and deep sea basin sediments off Uruguay (SW Atlantic). Int. J. Earth Sci. 88, 619–629.

Haese, R.R., 2006. The biogeochemistry of iron. In: Schulz, H.D., Zabel, M. (Eds.), Marine Geochemistry, 2nd Edition. Springer Berlin Heidelberg New York, 241-270.

Henkel, S., Strasser, M., Schwenk, T., Hanebuth, T.J.J., Hüsener, J., Arnold, G.L., Winkelmann, D., Formolo, M., Tomasini, J., Krastel, S., Kasten, S., 2011. An interdisciplinary investigation of a recent submarine mass transport deposit at the continental margin off Uruguay. Geochem. Geophys. Geosyst., 12, Q08009.

Henkel, S., Schwenk, T., Hanebuth, T.J.J., Strasser, M., Riedinger, N., Formolo, M., Tomasini, J., Krastel, S., Kasten, S., 2012. Pore water geochemistry as a tool for identifying and dating recent mass-transport deposits. In: Yamada, Y., Kawamura, K., Ikehara, K., Ogawa, Y., Urgeles, R., Mosher, D., Chaytor, J., Strasser, M. (Eds.), Submarine Mass Movements and Their Consequences. Advances in Natural and Technological Hazards Research, Vol. 31, 87-97.

Hensen, C., Zabel, M., Pfeifer, K., Schwenk, T., Kasten, S., Riedinger, N., Schulz, H.D., Boetius, A., 2003. Control of sulfate pore water profiles by sedimentary events and the significance of anaerobic oxidation of methane for the burial of sulfur in marine sediments. Geochim. Cosmochim. Acta 67, 2631–2647.

Hinrichs, K.-U., Hayes, J.M., Sylva, S.P., Brewer, P.G., DeLong, E.F., 1999. Methane-consuming archaebacterial in marine sediments. Nature 398, 802-805.

Hsu, T.-W., Jiang, W.-T., Wang, Y., 2014. Authigenesis of vivianite as influenced by methane-induced sulfidization in cold-seep sediments off southwestern Taiwan. J. Asian Earth Sci. 89, 88-97.

Jahnke, R.A., Emerson, S.R., Roe, K.K., Burnett, W.C., 1983. The present day formation of apatite in Mexican continental margin sediments. Geochim. Cosmochim. Acta 47, 259–266.

Jilbert, T. Slomp, C.P., 2013. Iron and manganese shuttles control the formation of authigenic phosphorus minerals in the euxinic basins of the Baltic Sea. Geochim. Cosmochim. Acta 107, 155-169.

Jørgensen, B.B., Kasten, S., 2006. Sulphur cycling and methane oxidation. In: Schulz, H.D., Zabel, M. (Eds.), Marine Geochemistry, 2nd Edition. Springer Berlin Heidelberg New York, 271-309.

Joshi, S.R., Kukkadapu, R.K., Burdige, D.J., Bowden, M.E., Sparks, D.L., Jaisi, D.P., 2015. Organic matter remineralization predominates phosphorus cycling in the mid-bay sediments in the Chesapeake Bay. Environ. Sci. Technol. 49, 5887-5896.

Kasten, S., Freudenthal, T., Gingele, F.X., Schulz, H.D., 1998. Simultaneous formation of iron-rich layers at different redox boundaries in sediments of the Amazon deep-sea fan. Geochim. Cosmochim. Acta 62, 2253–2264.

Kasten, S., Zabel, M., Heuer, V., Hensen, C., 2003. Processes and signals of nonsteady-state diagenesis in deep-sea sediments and their pore waters, In: Wefer, G., Mulitza, S., Ratmeyer, V. (Eds.), The South Atlantic in the Late Quaternary. Springer Berlin Heidelberg New York, 431-459.

Kim, D., Schuffert, J.D., Kastner, M., 1999. Francolite authigenesis in California continental slope sediments and its implication for the marine P cycle. Geochim. Cosmochim. Acta 63, 3477–3485.

Kostka, J.E., Luther III, G.W., 1994. Partitioning and speciation of solid phase iron in saltmarsh sediments. Geochim. Cosmochim. Acta 58, 1701–1710.

Kraal, P., Slomp, C., Forster, A., Kuypers, M.M.M., Sluijs, A., 2009. Pyrite oxidation during sample storage determines phosphorus fractionation in carbonate-poor anoxic sediments. Geochim. Cosmochim. Acta 73, 3277-3290.

Kraal, P., Slomp, C., 2014. Rapid and extensive alteration of phosphorus speciation during oxic storage of wet sediment samples. PloS ONE 9(5); e96859. doi:10.1371/journal.pone.0096859.

Kraal, P., Dijkstra, N., Behrends, T., Slomp, C.P. (2017) Phosphorus burial in sediments of the sulfidic deep Black Sea: Key roles for adsorption by calcium carbonate and apatite authigenesis. Geochim. Cosmochim. Acta 204, 140-158.

Küster-Heins, K., de Lange, G.J., Zabel, M., 2010a. Benthic phosphorus and iron budgets for three NW African slope sediments: A balance Approach. Biogeosci. 7, 469-480.

Küster-Heins, K., Steinmetz, E., de Lange, G.J., Zabel, M., 2010b. Phosphorus cycling in marine sediments from the continental margin off Namibia. Mar. Geol. 274, 95-106.

Li, W., Joshi, S.R., Hou, G., Burdige, D.J., Sparks, D.L., Jaisi, D.P., 2015. Characterizing phosphorus speciation of Chesapeake Bay sediments using chemical extraction, ^{31}P NMR, and X-ray absorption fine structure spectroscopy. Environ. Sci. Technol. 49, 203-211.

Lijklema, L., 1980. Interaction of orthophosphate with iron(III) and aluminium hydroxides. Environ. Sci. Technol. 14, 537-541.

Lovley, D.R., Phillips, E.J.P., 1988. Novel mode of microbial energy metabolism: organic carbon oxidation coupled to dissimilatory reduction of iron or manganese. Appl. Environ. Microbiol. 54, 1472-1480.

Martens, C.S., Berner, R.A., Rosenfeld, J.K., 1978. Interstitial water chemistry of anoxic Long Island Sound sediments. 2. Nutrient regeneration and phosphate removal. Limnol. Oceanogr. 23, 605-617.

März, C., Hoffmann, J., Bleil, U., de Lange, G.J., Kasten, S., 2008. Diagenetic changes of magnetic and geochemical signals by anaerobic methane oxidation in sediments of the Zambezi deep-sea fan (SW Indian Ocean). Mar. Geol. 255, 118-130.

McManus, J., Berelson, W.M., Coale, K., Johnson, K., Kilgore, T.E., 1997. Phosphorus regeneration in continental margin sediments. Geochim. Cosmochim. Acta 61, 2891-2907.

Meister, P., McKenzie, J.A., Vasconcelos, C., Bernasconi, S., Frank, M., Gutjahr, M., Schrag, D.P., 2007. Dolomite formation in the dynamic deep biosphere: results from the Peru Margin. Sedimentology 54, 1007-1031.

Milucka, J., Ferdelman, T.G., Polerecky, L., Franzke, D., Wegener, G., Schmid, M., Lieberwirth, I., Wagner, M., Widdel, F., Kuypers, M.M.M., 2012. Zero-valent sulphur is a key intermediate in marine methane oxidation. Nature 491, 541-546.

Mucci, A., Richard, L.-F., Lucotte, M., Giugnard, C., 2000. The differential geochemical behaviour of arsenic and phosphorus in the water column and sediments of the Saguenay Fjord Estuary, Canada. Aquat. Geochem. 6, 293-324.

Nembrini, G.P., Capobianco, J.A., Viel, M., Williams, A.F., 1983. A Mössbauer and chemical study of the formation of vivianite in sediments of Lago Maggiore (Italy). Geochim. Cosmochim. Acta 47, 1459-1464.

Nriagu, J.O., 1972. Stability of vivianite and ion-pair formation in the system Fe3(PO4)2–H3PO4–H2O. Geochim. Cosmochim. Acta 36, 459–470.

Omelon, S.J., Grynpas, M.D., 2003. Relationships between polyphosphate chemistry, biochemistry and apatite biomineralization. Chem. Rev. 108, 4694-4715.

Oni, O., Miyatake, T., Kasten, S., Richter-Heitmann, T., Fischer, D., Wagenknecht, L., Kulkarni, A., Blumers, M., Shylin, S.I., Ksenofontov, V., Costa, B.F.O., Klingelhöfer, G., Friedrich, M.W., 2015. Distinct microbial populations are tightly linked to the profile of dissolved iron in the methanic sediments of the Helgoland mud area, North Sea. Front. Microbiol. 6, 365. doi:10.3389/fmicb.2015.00365.

Oxmann, J.F., Schwendenmann, L., 2014. Quantification of octacalcium phosphate, authigenic apatite and detrital apatite in coastal sediments using differential dissolution and standard addition. Ocean. Sci. 10, 571-585.

Parkhurst, D.L., Appelo, C.A.J., 2013, Description of input and examples for PHREEQC version 3 – A computer program for speciation, batch-reaction, one-dimensional transport,

and inverse geochemical calculations: U.S. Geological Survey Techniques and Methods 6, 497 p.

Pierre, C., Blanc-Valleron, M.-M., Caquineau, S., März, C., Ravelo, A.C., Takahashi, K., Alvarez Zarikian, C., 2016. Mineralogical, geochemical and isotopic characterization of authigenic carbonates from the methane-bearing sediments of the Bering Sea continental margin (IODP Expedition 323, Sites U1343–U1345). Deep-Sea Res II 125-126, 133-144.

Poulton, S.W., Krom, M.D., Raiswell, R., 2004. A revised scheme for the reactivity of iron (oxyhydr)oxide minerals towards dissolved sulphide. Geochim. Cosmochim. Acta 68, 3703–3715.

Pratesi, G., Cipriana, C., Guili, G., Birch, W.D., 2003. Santabarbaraite: a new amorphous phosphate mineral. Eur. J. Mineral. 15, 185–192.

Reed, D.C., Gustafsson, B.G., Slomp, C.P., 2016. Shelf-to-basin iron shuttling enhances vivianite formation in deep Baltic Sea sediments. Earth Planet. Sci. Lett. 434, 241-251.

Riedinger, N., Pfeifer, K., Kasten, S., Garming, J.F.L., Vogt, C., Hensen, C., 2005. Diagenetic alteration of magnetic signals by anaerobic oxidation of methane related to a change in sedimentation rate. Geochim. Cosmochim. Acta 69, 4117–4126.

Riedinger, N., Formolo, M.J., Lyons, T.W., Henkel, S., Beck, A., Kasten, S. (2014) An inorganic geochemical argument for coupled anaerobic oxidation of methane and iron reduction in marine sediments. Geobiol. 12, 172-181.

Riedinger, N., Brunner, B., Krastel, S., Arnold, G.L., Wehrmann, L., Formolo, M.J., Beck, A., Bates, S.M., Henkel, S., Kasten, S., Lyons, T.W. (2017) Sulfur cycling in an iron oxide-dominated, dynamic marine depositional system: The Argentine continental margin. Frontiers in Earth Science, 5(33).

Ruttenberg, K.C., 1992. Development of a sequential extraction method for different forms of phosphorus in marine sediments. Limnol. Oceanogr. 37, 1460–1482.

Ruttenberg, K.C., Berner, R.A., 1993. Authigenic apatite formation and burial in sediments from non-upwelling, continental margin environments. Geochim. Cosmochim. Acta 57, 991–1007.

Ruttenberg, K.C., 2003.The global phosphorus cycle. In: Holland, H.D., Turekian, K.K. (Eds.), Treatise on Geochemistry, 8. Elsevier, pp. 585–643.

Schefuβ, E., Kuhlmann, H., Mollenhauer, G., Prange, M., Pätzold, J., 2011. Forcing of wet phases in southeast Africa over the past 17,000 years. Nature 480, 509-512.

Schenau, S.J., de Lange, G.J., 2000. A novel chemical method to quantify fish debris in marine sediments. Limnol. Oceanogr. 45, 963–971.

Schenau, S.J., Slomp, C.P., de Lange, G.J., 2000. Phosphogenesis and active phosphorite formation in sediments from the Arabian Sea oxygen minimum zone. Mar. Geol. 169, 1–20.

Schuffert, J.D., Kastner, M., Jahnke, R.A., 1998. Carbon and phosphorus burial associated with modern phosphorite formation. Mar. Geol. 146, 21–31.

Schulz, H.D., 2006. Quantification of early diagenesis: dissolved constituents in pore water and signals in the solid phase, In: Schulz, H.D., Zabel, M. (Eds.), Marine Geochemistry, 2nd Edition. Springer Berlin Heidelberg New York, 73–124.

Schulz, H.N., Schulz, H.D., 2005. Large sulfur bacteria and the formation of phosphorite. Science 307, 416-418.

Schulz, H.D., Dahmke, A., Schinzel, U., Wallmann, K., Zabel, M., 1994. Early diagenetic processes, fluxes, and reaction rates in sediments of the South Atlantic. Geochim. Cosmochim. Acta 58, 2041–2060.

Shanmugam, G., Moiola, R.J., Damuth, J.E., 1985. Eustatic control of submarine fan development. In: Bouma, A.H., Normark, W.R., Barnes, N.E. (Eds.), Submarine Fans and Related Turbidite Systems, Springer-Verlag, New York, 23-28.

Sheldon, R.P., 1981. Ancient marine phosphorites. Ann. Rev. Earth Planet. Sci. 9, 251–284.

Sivan, O., Shusta, S.S., Valentine, D.L., 2016. Methanogens rapidly transition from methane production to iron reduction. Geobiol. 14, 190-203.

Slomp, C.P., van der Gaast, S.J., van Raaphorst,W., 1996a. Phosphorus binding by poorly crystalline iron oxides in North Sea sediments. Mar. Chem. 52, 55–73.

Slomp, C.P., Epping, E.H.G., Helder, W., van Raaphorst, W., 1996b. A key role for iron-bound phosphorus in authigenic apatite formation in North Atlantic continental

platform sediment. J. Mar. Res. 54, 1179–1205.

Slomp, C.P., Mort, H.P., Jilbert, T., Reed, D.C., Gustafsson, B.G., Wolthers, M., 2013. Coupled dynamics of iron and phosphorus in sediments of an oligotrophic coastal basin and the impact of anaerobic oxidation of methane. PLoS ONE 8, e62386, doi:10.1371/journal.pone.0062386.

Sundby, B., Gobeil, C., Silverberg, N., Mucci, A., 1992. The phosphorus cycle in coastal marine sediments. Limnol. Oceanogr. 37, 1129-1145.

Taldenkova, E., Bauch, H.A., Gottschalk, J., Nikolaev, S., Rostovtseva, Y., Pogodina, I., Ovsepyan, Y., Kandiano, E., 2010. History of ice-rafting and water mass evolution at the northern Siberian continental margin (Laptev Sea) during Late Glacial and Holocene times. Quat. Sci. Rev. 29, 3919-3935.

Van Cappellen, P., Berner, R.A., 1988. A mathematical model for the early diagenesis of phosphorus and fluorine in marine sediments: apatite precipitation. Am. J. Sci. 288, 289-333.

Van Cappellen, P., Berner, R.A., 1991. Fluorapatite crystal growth from modified seawater solutions. Geochim. Cosmochim. Acta 55, 1219-1234.

Van der Lubbe, H.J.L., Tjallingij, R., Prins, M.A., Brummer, G;-J., Jung, S.J.A., Kroon, D., Schneider, R.R., 2014. Sedimentation patterns off the Zambezi River over the last 20,000 years. Mar. Geol. 355, 189-201.

Wang, X., Liu, F., Tan, W., Li, W., Feng, X., Sparks, D.L., 2013. Characteristics of phosphate adsorption-desorption onto ferrihydrite: comparison with well-crystalline Fe (hydr)oxides. Soil Sci. 178, 1-11.

Wehrmann, L.M., Ockert, C., Mix, A.C., Gussone, N., Teichert, B.M.A., Meister, P., 2016. Repeated occurrences of methanogenic zones, diagenetic dolomite formation and linked silicate alteration in southern Bering Sea sediments (Bowers Ridge, IODP Exp. 323 Site U1341). Deep-Sea Res. II 125-126, 117-132.

Wiles, E., Green, A.N., Watkeys, M.K., Jokat, W., 2017. Zambezi continental margin: compartmentalized sediment transfer routes to the abyssal Mozambique Channel. Mar. Geophys. Res. 38, 227-240.

Tables:

Table 1: Names, longitudes/latitudes, research cruises, water depths, core lengths, and related publications of the four studied sediment cores.

Table 2: Identification of the sampled pore waters selected for the geochemical inverse models performed in PHREEQC.

Table 3: Predicted distribution of P in the initial and final pore waters and in the solid phases considered in the two inverse models performed in PHREEQC. In Model 1, the initial water is above the SMT, and the final water within the SMT. In Model 2, the initial water is within the SMT, and the final water is below the SMT.

Figures:

Figure 1: Global map (upper right) with catchment areas of the Amazon, Rio de la Plata and Zambezi rivers (dark grey), and zoomed insets of the coring sites (a) off the Amazon (GeoB 1514), (b) off the Rio de La Plata (GeoB 6223 and 6308), and (c) off the Zambezi (GeoB 9309). Dashed grey lines mark the 200 m water depth contour, solid grey lines mark the 1000 m, 2000 etc. water depth contours.

Figure 2: Pore water concentrations of SO_4^{2-} (mmol/l), HS^- (µmol/l), Fe^{2+} (µmol/l), PO_4^{3-} (µmol/l) and Fe (oxyhydr)oxides (FeOx, sum of Fe_{asc} and Fe_{dith} fractions)(wt% of dry sediment) in cores GeoB 1514, 6223, 6308 and 9309. Grey bar indicates sulphidic zone within the SMT.

Figure 3: Pore water concentrations of Ca^{2+} (mmol/l) and F^- (µmol/l) in cores GeoB 1514, 6223, 6308 and 9309 (no F^- data available for 9309). Grey bar indicates sulphidic zone within the SMT.

Figure 4: Contents of Fe_{asc} (amorphous/poorly crystalline Fe (oxyhydr)oxides; filled circles) and Fe_{dith} (crystalline Fe oxides; open circles) fractions (no data for GeoB 1514) in µmol/g of dry sediment. Grey bar indicates sulphidic zone within the SMT.

Figure 5: Contents of different extracted P fractions (P_{loose} = hydroxyapatite, octocalcium-phosphate; P_{Fe} = Fe-bound P; P_{CFA} = carbonate fluorapatite; P_{FA} = fluorapatite; P_{org} = organic P) in µmol/g of dry sediment at the four studied sites.

Figure 6: Contents of different extracted P fractions (P_{loose} = hydroxyapatite, octocalcium-phosphate; P_{Fe} = Fe-bound P; P_{CFA} = carbonate fluorapatite; P_{FA} = fluorapatite; P_{org} = organic P) in rel% of P_{total} at the four studied sites.

Figure 7: PHREEQC calculations of pore water saturation indices (SI) for vivianite and hydroxyapatite at sites GeoB 1514, 6223, 6308 and 9309. Grey bar indicates sulphidic zone within the SMT.

Figure 8: Estimated amounts of mineral dissolution and precipitation in the inverse models performed in PHREEQC for sites GeoB 1514, 6223 and 6308.

Figure 9: Schematic illustration of relevant depositional and diagenetic processes leading to iron-phosphorus cycling in continental margin settings affected by drastic decreases in sedimentation rates during (top) and after (bottom) the last deglaciation.

Gravity core	Cruise	Core location	Water depth	Core length	Reference
GeoB 1514	M16/2	5°08.4´N, 46°34.6´W (Amazon deep-sea fan)	3,509 m	710 cm	Kasten et al. (1998)
GeoB 6223	M46/2	35°44.42´S, 49°40.86´W (Rio de La Plata depocentre)	4,280 m	867 cm	Riedinger et al. (2005)
GeoB 6308	M46/2	39°10.00´S, 53°08.70´W (Rio de La Plata depocentre)	3,620 m	1,166 cm	Riedinger et al. (2005)
GeoB 9309	M63/1	18°55.8'S, 37°30.7'E (Zambezi deep-sea fan)	1,219 m	625 cm	März et al. (2008)

Table 1

Model	Site	Initial water (depth, cm)	Final water (depth, cm)	Vertical distance between pore waters (cm)
1. Within SMT	1514	15	510	495
	6223	10	510	490
	6308	10	635	625
2. Below SMT	1514	635	680	45
	6223	535	610	75
	6308	635	735	100

Table 2

Model	Site	Pore water depth (cm)	Ferrihydrite-sorbed P (%)	Vivianite (%)	CFA (%)	P(aq) (%)
1	1514	15 (initial)	99.997	0.000	0.000	0.003
		510 (final)	9.132	7.322	83.317	0.229
	6223	10 (initial)	9.977	0.000	0.000	0.023
		510 (final)	9.492	6.666	83.434	0.407
	6308	10 (initial)	99.978	0.000	0.000	0.022
		635 (final)	11.632	4.681	83.444	0.243
2	1514	635 (initial)	93.297	0.000	0.000	6.703
		680 (final)	0.000	96.157	0.000	3.843
	6223	535 (initial)	98.049	0.000	0.000	1.951
		610 (final)	6.973	10.801	81.591	0.635
	6308	635 (initial)	75.164	0.000	0.000	25.836
		735 (final)	0.000	87.571	0.000	12.429

Table 3

Highlights

- Release of phosphate at sulphate-methane transitions (SMT) of continental margin sediments.
- Carbonate fluorapatite (CFA) formation within the SMT, but not below it.
- Pore water phosphate drawdown below SMT due to Fe(II) phosphate formation.
- Phosphate diagenesis controlled by fixation of SMT due to low sedimentation rate on deep-sea fans following Holocene sea level rise.

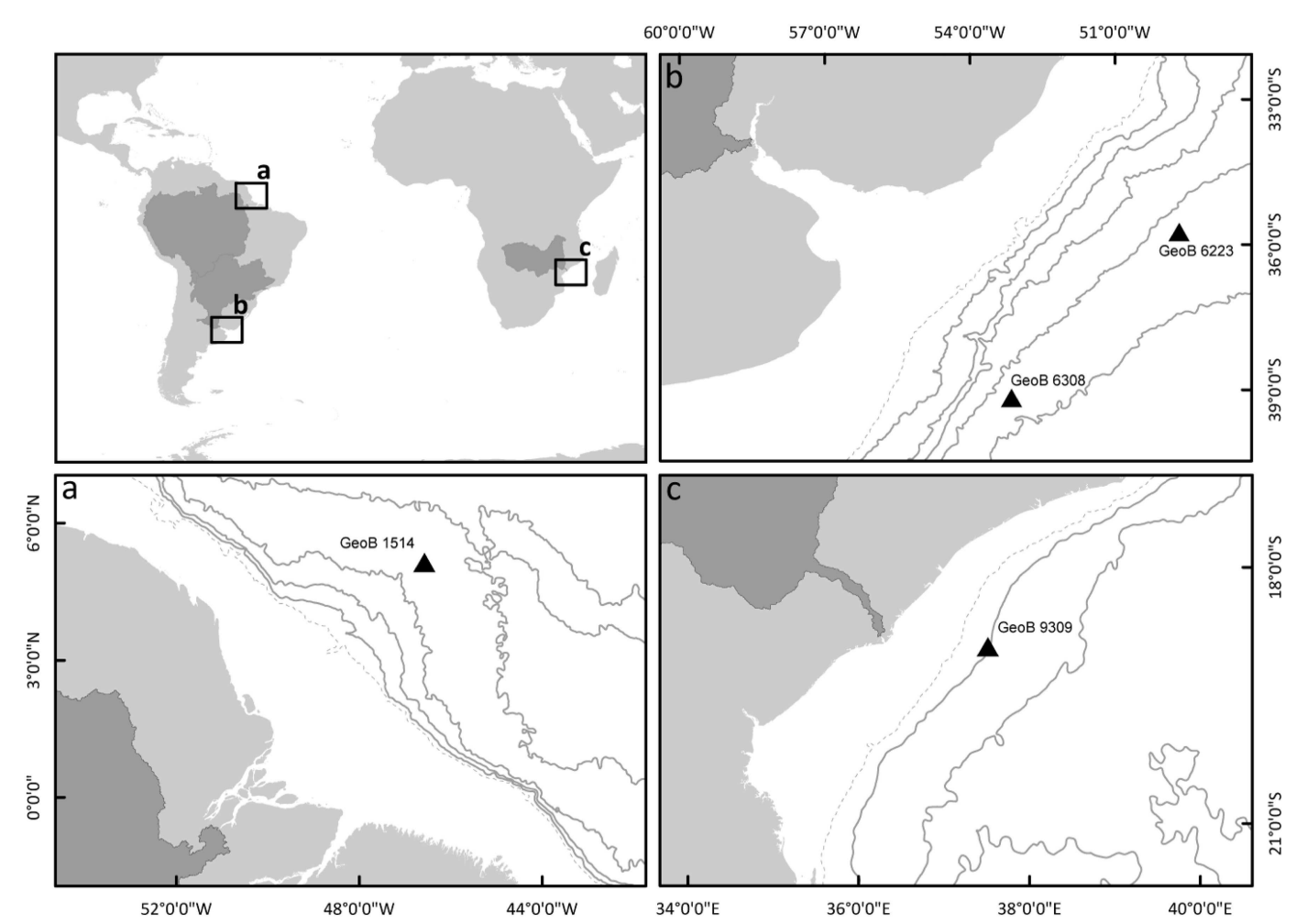
a
b
c
60°0'0"W
57°0'0"W
54°0'0"W
51°0'0"W
33°0'0"S
36°0'0"S
39°0'0"S
GeoB 6223
GeoB 6308
6°0'0"N
3°0'0"N
0°0'0"
GeoB 1514
52°0'0"W
48°0'0"W
44°0'0"W
18°0'0"S
21°0'0"S
GeoB 9309
34°0'0"E
36°0'0"E
38°0'0"E
40°0'0"E

Figure 1

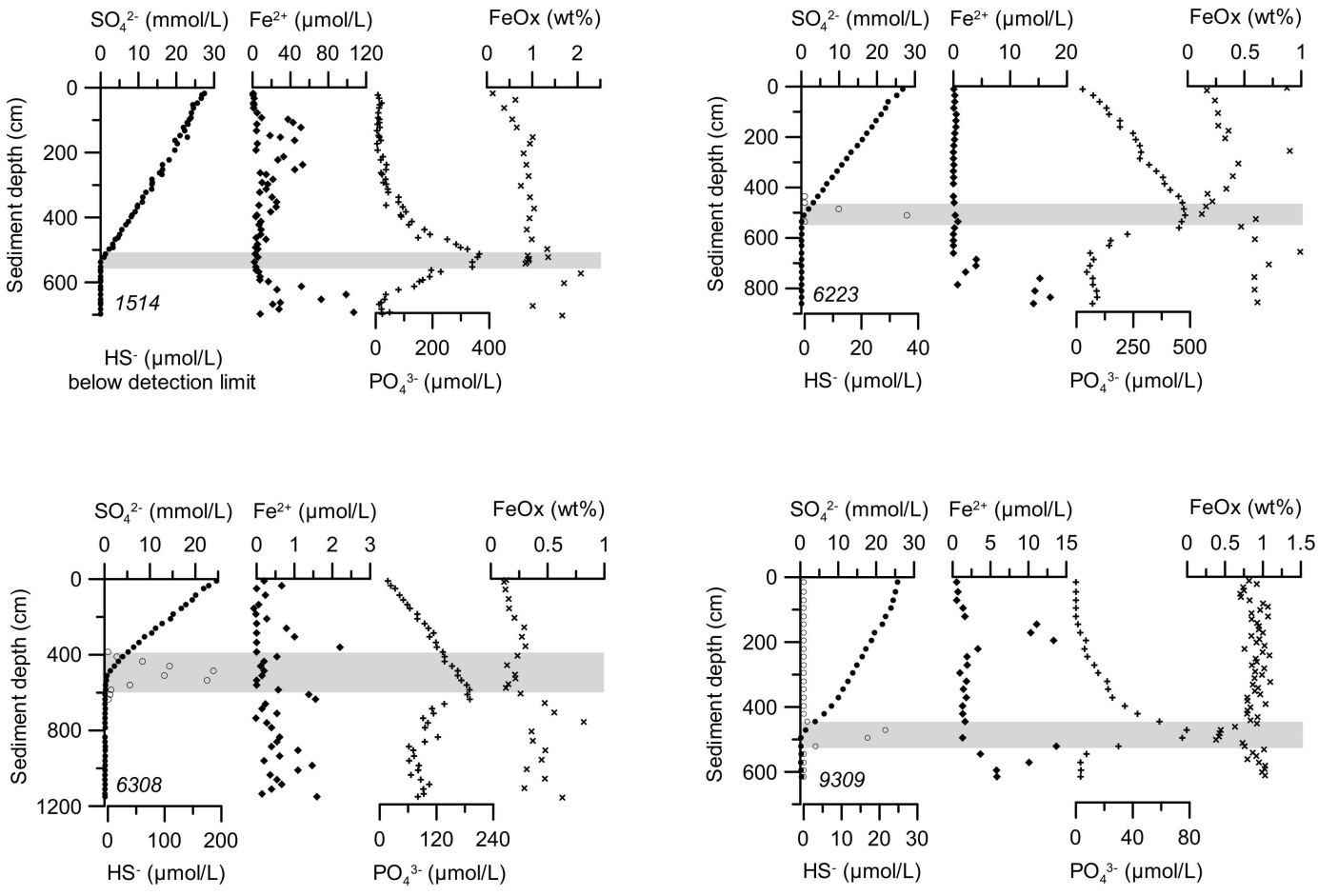
SO4 2- (mmol/L)
Fe2+ (µmol/L)
FeOx (wt%)
Sediment depth (cm)
1514
HS- (µmol/L)
below detection limit
PO4 3- (µmol/L)
6223
6308
9309

Figure 2

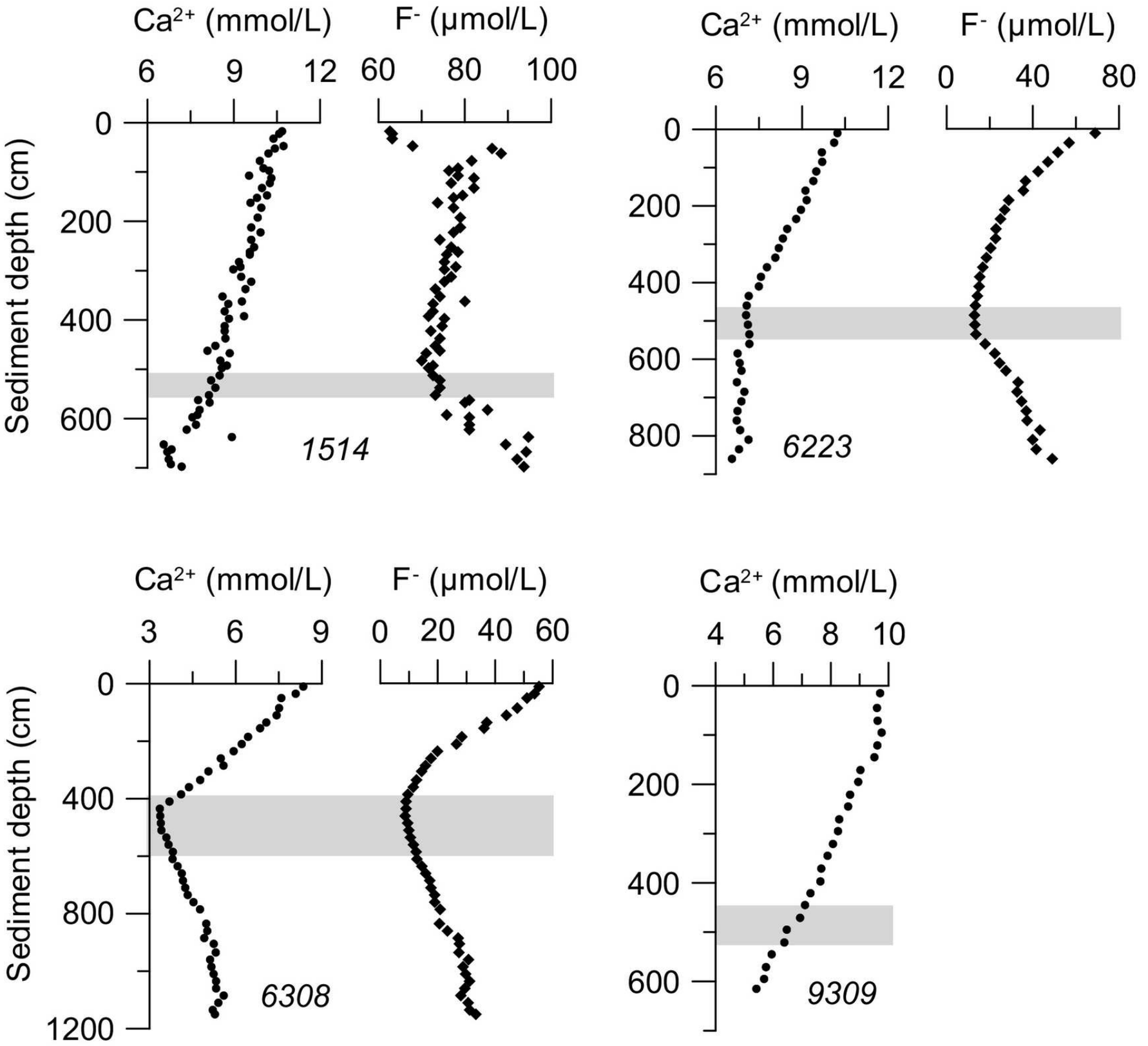

Figure 3

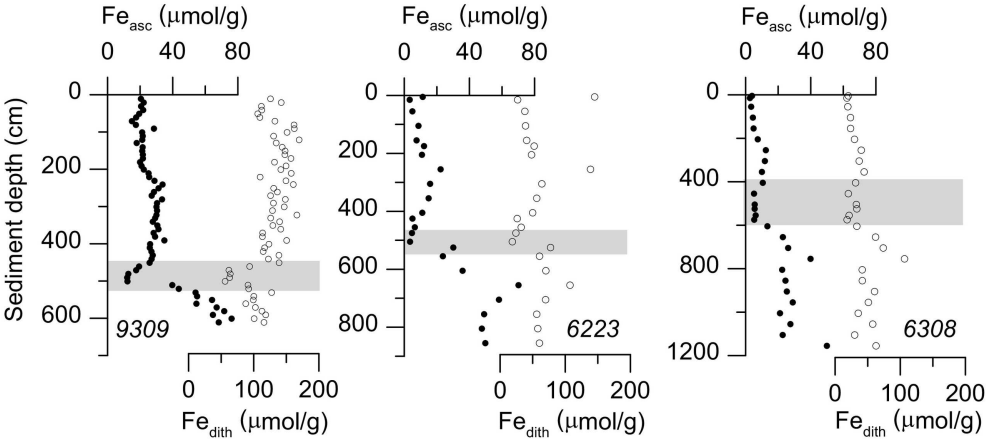
Fe$_{asc}$ (μmol/g)
0
40
80
Sediment depth (cm)
0
200
400
600
9309
Fe$_{dith}$ (μmol/g)
0
100
200
Fe$_{asc}$ (μmol/g)
0
40
80
0
200
400
600
800
6223
Fe$_{dith}$ (μmol/g)
0
100
200
Fe$_{asc}$ (μmol/g)
0
40
80
0
400
800
1200
6308
Fe$_{dith}$ (μmol/g)
0
100
200

Figure 4

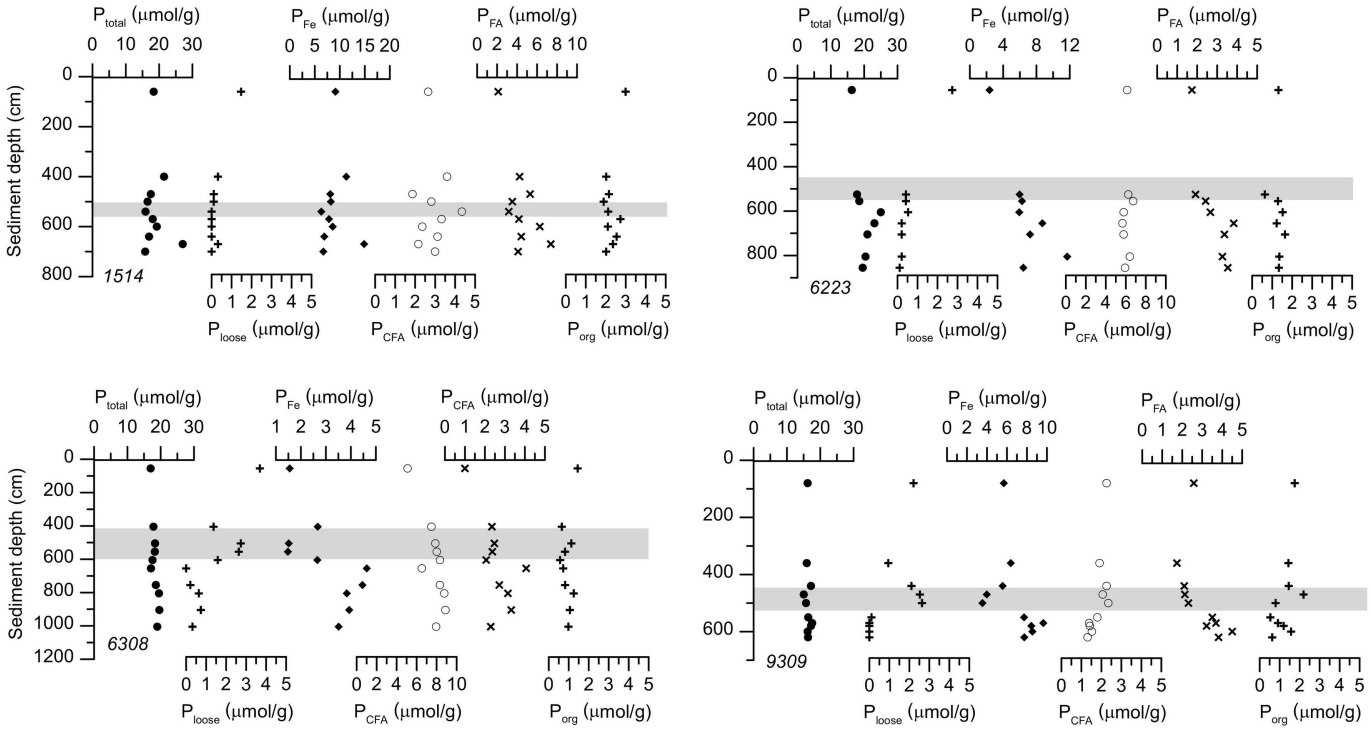
Sediment depth (cm)
P_total (μmol/g)
P_Fe (μmol/g)
P_FA (μmol/g)
P_CFA (μmol/g)
P_loose (μmol/g)
P_org (μmol/g)
1514
6223
6308
9309

Figure 5

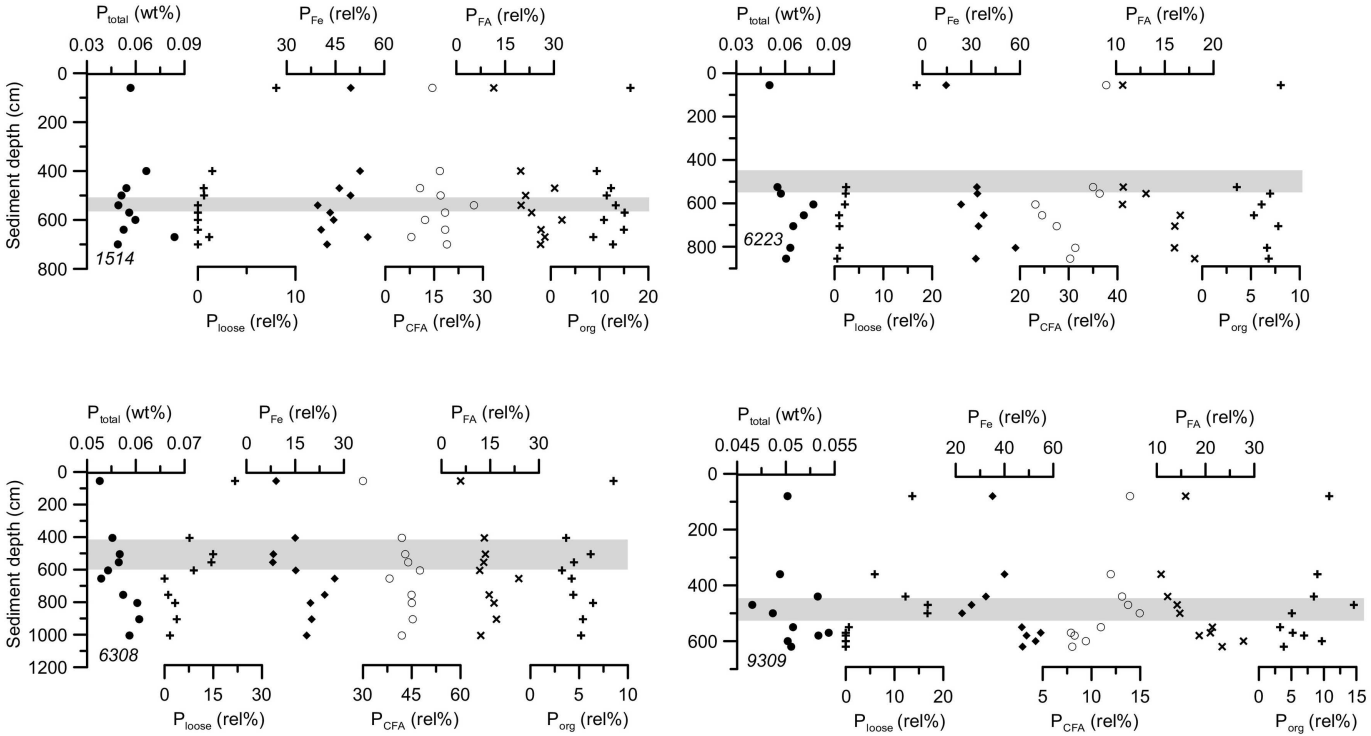
Sediment depth (cm)
P_total (wt%)
P_Fe (rel%)
P_FA (rel%)
P_loose (rel%)
P_CFA (rel%)
P_org (rel%)
1514
6223
6308
9309

Figure 6

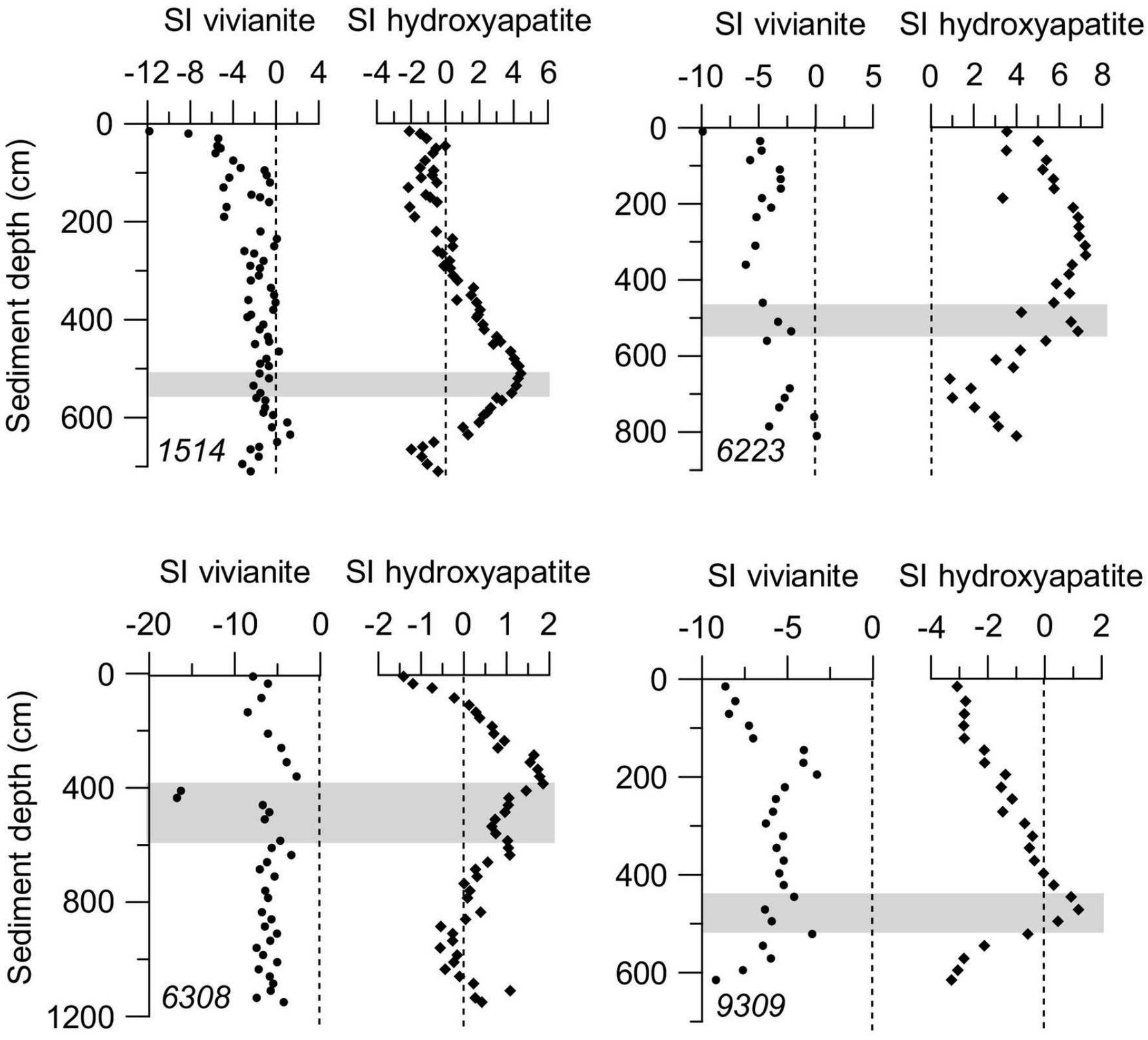
SI vivianite
SI hydroxyapatite
Sediment depth (cm)
1514
6223
6308
9309

Figure 7

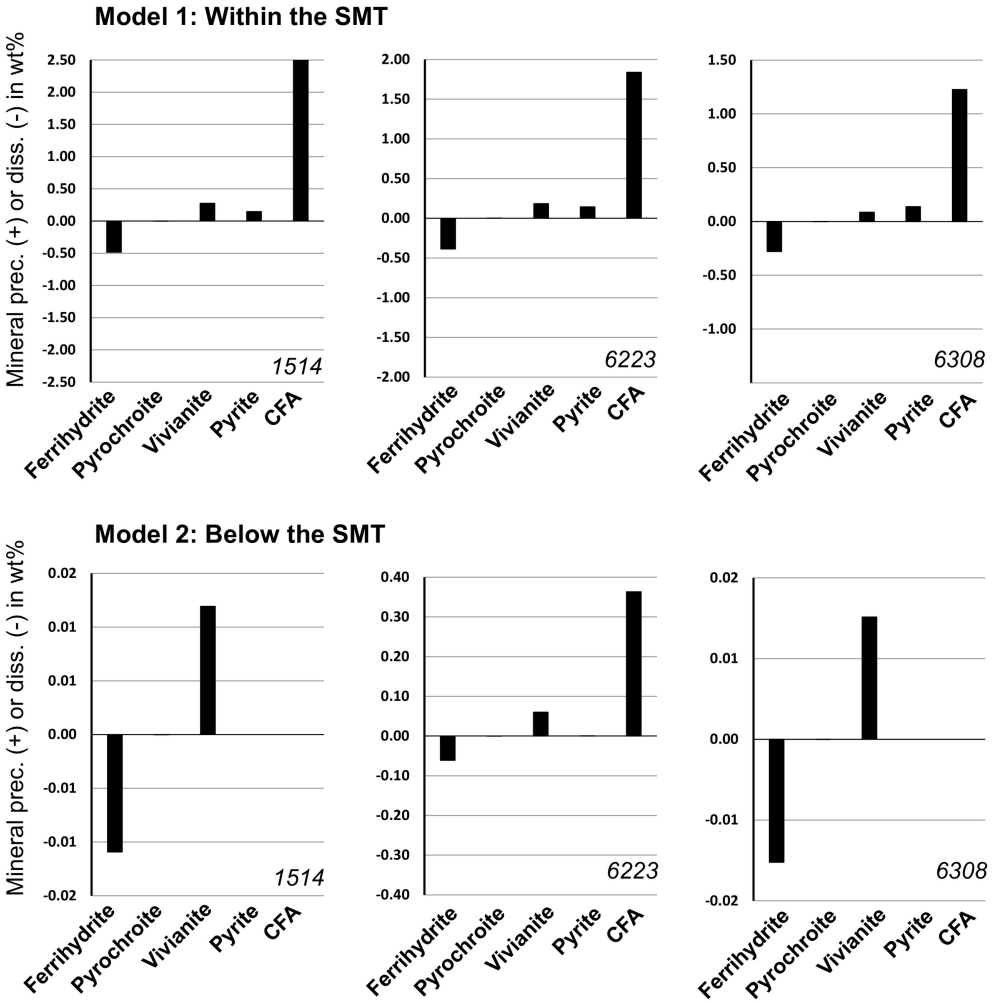
Model 1: Within the SMT
Mineral prec. (+) or diss. (-) in wt%
2.50
2.00
1.50
1.00
0.50
0.00
-0.50
-1.00
-1.50
-2.00
-2.50
1514
6223
6308
Ferrihydrite
Pyrochroite
Vivianite
Pyrite
CFA
Model 2: Below the SMT
Mineral prec. (+) or diss. (-) in wt%
0.02
0.01
0.00
-0.01
-0.02
0.40
0.30
0.20
0.10
-0.10
-0.20
-0.30
-0.40
1514
6223
6308
Ferrihydrite
Pyrochroite
Vivianite
Pyrite
CFA

Figure 8

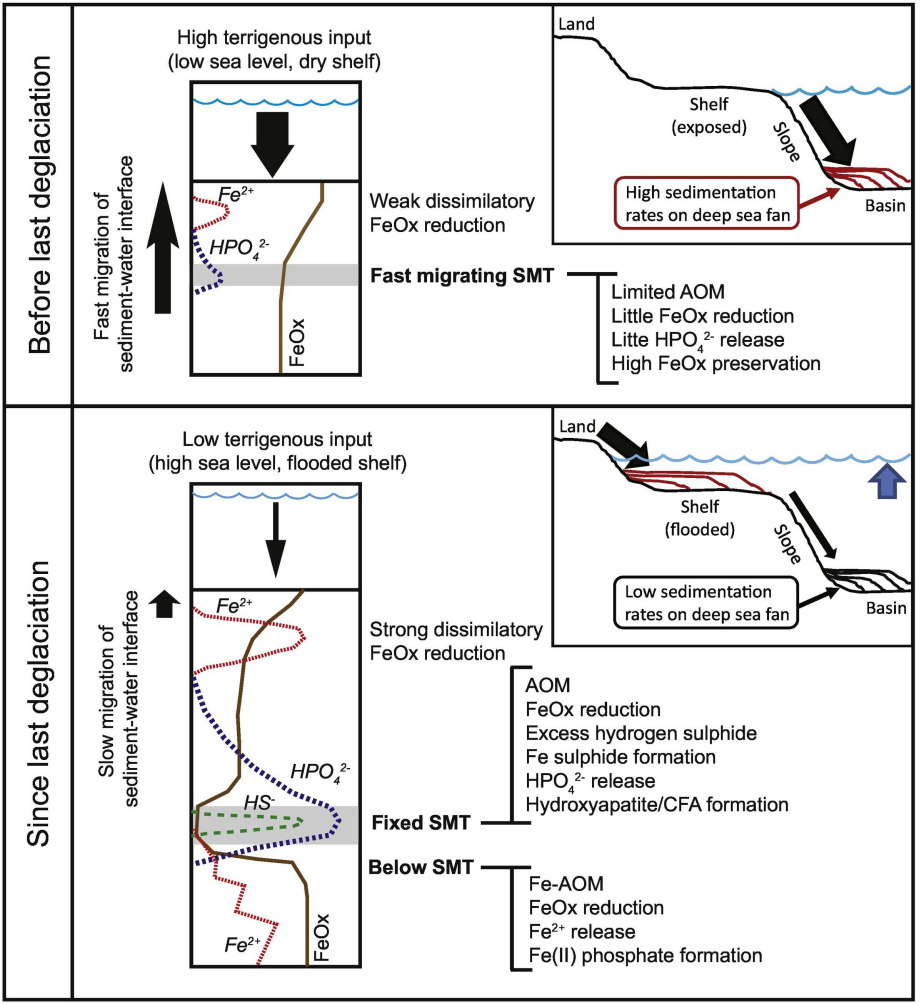
Before last deglaciation
High terrigenous input
(low sea level, dry shelf)
Fast migration of
sediment-water interface
Fe2+
HPO4 2-
FeOx
Weak dissimilatory
FeOx reduction
Fast migrating SMT
Limited AOM
Little FeOx reduction
Litte HPO4 2- release
High FeOx preservation
Land
Shelf
(exposed)
Slope
High sedimentation
rates on deep sea fan
Basin
Since last deglaciation
Low terrigenous input
(high sea level, flooded shelf)
Slow migration of
sediment-water interface
Fe2+
HPO4 2-
HS-
Fe2+
FeOx
Strong dissimilatory
FeOx reduction
AOM
FeOx reduction
Excess hydrogen sulphide
Fe sulphide formation
HPO4 2- release
Hydroxyapatite/CFA formation
Fixed SMT
Below SMT
Fe-AOM
FeOx reduction
Fe2+ release
Fe(II) phosphate formation
Land
Shelf
(flooded)
Slope
Low sedimentation
rates on deep sea fan
Basin

Figure 9